Chapter 8a

Computational investigation on the effect of the peptidomimetic inhibitors (NPT100-18A and NPT200-11) on the α-Synuclein and lipid membrane interactions

Computational investigation on the effect of the peptidomimetic inhibitors (NPT100-18A and NPT200-11) on the α-Synuclein and lipid membrane interactions

8a.1. Abstract:

PD is associated with α-Syn, a presynaptic protein that binds to cell membranes. The molecular pathophysiology of PD most likely begins with the binding of α-Syn to membranes. Recently, two peptidomimetic inhibitors (NPT100-18A and NPT200-11) were identified to potentially interact with α-Syn and affect the interaction of α-Syn with the membrane. In this study, the effect of the two peptidomimetic inhibitors on the α-Syn-membrane interaction was demonstrated. DFT calculations were performed for optimization of the two inhibitors, and the nucleophilicity (N) and electrophilicity (ω) of NPT100-18A and NPT200-11 were calculated to be 3.90 and 3.86 (N); 1.06 and 1.04 (ω) respectively. Using the docking tool (CB-dock2), the two α-Syn-peptidomimetic inhibitor complexes (α-Syn-NPT100-18A and α-Syn-NPT200-11) have been prepared. Then all-atom MD simulation was carried out on the α-Syn (control), α-Syn-NPT100-18A and α-Syn-NPT200-11 complex systems in presence of DOPE/DOPS/DOPC (5:3:2) lipid bilayer. From the conformational dynamics analysis, the 3-D structure of α-Syn was found to be stable, and the helices present in the regions (1-37) and (45–95) of α-Syn were found to be retained in the presence of the two peptidomimetic inhibitors. The electron density profile analysis revealed the binding modes of NAC and C-terminal region of α-Syn (in the presence of NPT200-11 inhibitor) with lipid membrane are in the close vicinity from the lipid bilayer centre. Our findings in this study on α-Syn-membrane interactions may be useful for developing a new therapeutic approach for treating PD and other neurodegenerative disorders.

8a.2. Introduction:

PD, dementia with LB, and multiple system atrophy are together known as synucleinopathies, and it is thought that progressive buildup of the synaptic protein α-Syn (encoded by SNCA) plays a significant role in the pathogenesis of these diseases. There is presently no disease-modifying medication for the approximately 10 million people around the world who suffer from synucleinopathies [10, 485-487]. Although the exact mechanisms leading to pathological accumulation of α-Syn remain unclear, there is evidence to suggest that changes in the rate of synthesis play a role [488-491]. Accumulation and aggregation of α-Syn cause toxic oligomers to develop, which may spread from cell to cell in a manner similar to prion diseases [2, 133, 492-499]. Neurodegeneration may be facilitated by oligomers of α-Syn that vary greatly in

size, shape, and conformation. Oligomers of varied sizes have been suggested to be harmful in certain investigations, whereas greater molecular weight aggregates have been suggested in other studies [162, 500-502]. In recent studies, MD simulation and biophysical investigations have shown that α-Syn binding and subsequent penetration of the neuronal membrane are significant steps in this process, supporting the possibility that higher order α-Syn aggregates are hazardous [303,503-506]. Thus, it is suggested that interactions between α-Syn and lipids in the neuronal cell membrane constitute a crucial step in the oligomerization and cytotoxicity processes [31, 32]. As a result, methods for removing α-Syn from the membrane, accelerating breakdown and clearance, avoiding aggregation, or reducing α-Syn formation may be effective therapeutic approaches. In earlier research, antibodies [507], proteolytic enzymes [508], and small compounds [403] that reduce α-Syn fibrillation or aggregation were used to target α-Syn aggregates. A library of 34 peptidomimetic analogues was recently developed to aid in the targeting α-Syn. From the library, NPT100-18A was identified as the most promising by using *in silico* and biophysical approaches to create peptidomimetic molecules with a pyrimido-pyrazine scaffold [505, 32]. The NPT100-18A is suggested to interact with α-Syn in the membrane, limiting the production of harmful oligomers. Several *in vivo* experiments on cells with distinct α-Syn NPT100-18A ameliorated symptoms in transgenic models were carried out and supported by behavioural impairments and neurodegeneration studies that aid in targeting the early oligomerization of α-Syn on its association with the membrane; a promising therapeutic strategy for synucleinopathies [182]. NPT200-11, a novel substance with enhanced pharmacokinetic characteristics, was introduced. In terms of reduced α-Syn buildup, amelioration of neurodegenerative disease, and improvements in behavioural function, compound NPT200-11 continued to exhibit similar efficacy to compound NPT100-18A. Compound NPT200-11 is unquestionably the most effective small-molecule therapeutic candidate for treating α-Syn aggregation. NPT100-18A and NPT200-11 are two peptidomimetics that were developed to inhibit α-Syn oligomerization by interfering with membrane function. NPT100-18A, a cyclic peptidomimetic analogue to the 96KKDQLGK102 sequence of α-Syn that most usually binds to another α-Syn molecule during oligomerization, was created [182]. However, this peptidomimetic displayed inadequate blood-brain barrier penetration, restricted oral bioavailability, and other drawbacks that prevented its progress as a therapeutic option [509]. In this study, the effects of NPT200-11 and NPT100-18A on α-Syn neuropathology were evaluated using MD simulations. Our findings put forward the potential binding position of these two drugs, NPT100-18A and NPT200-11, on α-Syn. Also, the impact of these two drugs on the α-Syn and lipid membrane interactions at an atomistic level.

8a.3. Materials and Methods:

8a.3.1. Molecular Docking of the complexes (α-Synuclein-NPT100-18A and α-Synuclein-NPT200-11):

8a.3.1.1. Preparation of receptor molecule:

The micelle-bound human WT α-Syn monomeric structure, obtained from the RCSB Protein Data Bank [457], PDB ID 1XQ8 [442], was used as the receptor molecule for molecular docking.

8a.3.1.2. Preparation of Ligand:

Optimization of the initial structure of Inhibitors was calculated as observed in **Figure 8a.1**.

Figure 8a.1. *B3LYP+D3/def2-TZVP (/CPCM) calculated optimized structure of inhibitors (NPT100-18A and NPT200-11) considered in this study*

8a.3.2. Computational details:

Density functional theory (DFT) calculations were performed for geometry optimisation of the two inhibitors considered in this study without any constraint (NPT100-18A and NPT200-11, **Figure 8a.1**) using the B3LYP hybrid functional [287] in conjunction with the def2-TZVP basis set [288, 289]. The D3 version of Grimme's dispersion correction [290] and the conductor-like polarizable continuum model (CPCM) was employed to mimic the aqueous solvent environment [291] (B3LYP+D3/def2-TZVP (CPCM)) with dielectric constant ε = 80.0. Frequency calculations were carried out at the same level of theory in order to characterise the correct stationary ground state, and for all of them, minima were obtained with real vibrational frequencies. All calculations were carried out with Gaussian 16 version C.01 of the programme [292]. Natural bond orbital (NBO) analysis was carried out to understand the nature of the frontier molecular orbitals (MO) of these inhibitors as implemented in the Gaussian 16 programme in the B3LYP+D3/def2-TZVP (CPCM) environment [293]. The xyz coordinates

of NPT100-18A and NPT200-11 structures were then changed to PDB format using the Open Babel server [294].

8a.3.3. Preparation of the docked complexes:

The α-Syn protein retrieved from Protein Data Bank was then docked to the two peptidomimetic molecules (NPT100-18A and NPT200-11) using CB-Dock2, an online docking server. **Figure 8a.2** provides a diagrammatic illustration of the process of preparing the docked complex of the receptor molecule and the peptidomimetic molecules. The CB-dock2 server [240] has provided us with many models of complex structures. Among the model structures, the initial complex structure was chosen based on the number of binding pockets and docking score for further investigation.

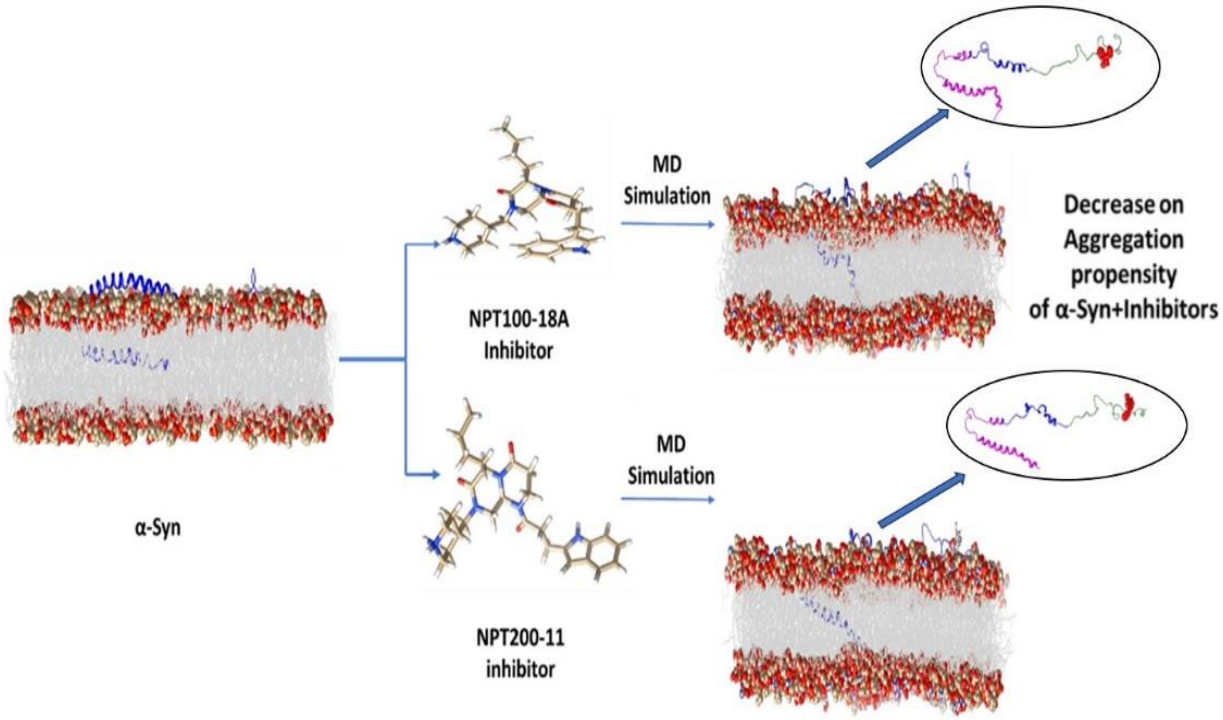

Figure 8a.2. *Schematic representation for the formation of docked complexes (α-Syn +NPT100-18A and α-Syn +NPT200-11)*

8a.3.4. Preparation of Simulation setup for α-Synuclein and docked complexes:

The WT α-Syn and docked complexes (α-Syn +NPT100-18A and α-Syn +NPT200-11) were uploaded to initiate the construction of the membrane bilayer using the CHARMM GUI server. The rest of the MD steps follows the module as mentioned in section **4.3.2.**

UCSF Chimera software alpha v.1.12 [298] was used to visualise this complex structure, separate the ligand and receptor, and save their coordinates in mol2 and PDB formats

[306]. The Antechamber protocol in xleap curated the chosen solution structure. Bcc charge, frcmod file, and complex systems in explicit and implicit solvation are required. Topology and coordinate files were then created for each system. The explicit solvation was used for complex system MD simulations.

8a.3.5. MD trajectory analysis:

Structural analysis of MD simulation for the α-Syn in the presence of peptidomimetic inhibitors (NPT100-18A and NPT200-11) were performed using the CPPTRAJ module [305] of AmberTools 18. Electrostatic potential energy was calculated to determine the interaction of these inhibitors with neighbouring residues of the protein. To assess the adopted simulation protocol, Area per lipid, membrane thickness, and Electron density profile analysis were analysed. The backbone RMSD of Cα atoms were analysed to study the stability and convergence of membrane-bound α-Syn in the presence of peptidomimetic inhibitors. To check the flexible and rigid regions of membrane-bound α-Syn in the presence of peptidomimetic inhibitors, RMSF were calculated from their corresponding trajectories obtained during MD simulation and plotted with respect to the residue index. The distance analysis between different regions of α-Syn in the presence of α-Syn were plotted. The secondary structural analysis of α-Syn in the presence of inhibitors were calculated using the Kabsch and Sander algorithm [295] and the percentage of secondary structure were calculated using YASARA software [258]. Intermolecular hydrogen bond analysis is used to analyse the proximity between the lipid bilayer and different regions of α-Syn in the presence of inhibitors.

8a.3.6. Principal Component Analysis (PCA) followed by free energy landscape (FEL) of MD trajectories

PCA defines high-amplitude coordinated motion in MD trajectories based on the eigenvectors of the mass-weighted covariance matrix (C) of atomic positional fluctuations [510], estimated on protein alpha carbons (Cα) using concatenated and single MD trajectories. PCA was used to make a free energy surface for the best-predicted a-Syn complex with and without inhibitors and to study how the shape of proteins changes [303, 304]. The entire trajectory inputs have been evaluated for PCA. Based on RMSD measurements, all systems stabilised after 40 ns. The MD simulation covariance matrix was computed and found its eigenvectors, which formed the comprehensive and mutually perpendicular reduced space basis set. When a molecular structure is projected onto a primary component space, each point uniquely matches a structure in the original coordinate system. Each primary component also has a weight that reflects its original structure's volatility. A few large-weight major components may identify the molecular

key structural characteristics. The free energy profiles for α-Syn were calculated in the presence of inhibitors using the likelihood of each point in a bin:

$$\Delta G = - k_B T \ln (\rho)$$

In this study, Amber's CPPTRAJ module [297] was used to perform PCA.

8a.3.7. Binding Free Energy (BFE) Calculations:

FastDRH (http://cadd.zju.edu.cn/fastdrh/), a web server to predict the Binding Free Energy (BFE) and was used to calculate the BFE of the α-Syn in the presence of inhibitor complexes based on computational docking and Generalized-Born surface area continuum solvation (MM/GBSA) methods, [262]. The overall BFE for the NPT100-18A+ α-Syn and NPT200-11+ α-Syn complexes were determined along with the other derived components (VDW, ELE, GB and SA) contributing to the overall BFE of the two complexes.

8a.4. Results and Discussions:

8a.4.1. Parameterization of compounds NPT100-18A and NPT200-11:

To interpret the charge distribution and most probable coupling intersystem interaction of these inhibitors with neighbouring residues a molecular electrostatic potential map (MESP) contour can be considered as a good descriptor, as tabulated in **Table 8a.1** and shown in **Figure 8a.3**. DFT was chosen to interpret electron density for the stationary states from ground state geometry optimization for all the systems. In **Table 8a.1**, for both the inhibitors (NPT100-18A and NPT200-11) the negative region is partially delocalized between the carbon-carbon double bond and over the C=O fragment. The MESP is widely used as a reactivity map in displaying probable electrophilic interaction, hydrogen bonding and possible secondary interaction in biological systems [511, 512].

In addition, the relative electron donation and acceptance ability of a particular molecule can be considered a fundamental property as it governs its key reactivity profile. Based on that, the energies of the five first highest occupied and unoccupied MO (HOMO and LUMO respectively) were characterized for NPT100-18A and NPT200-11 by the NBO partitioning scheme [293, 513] (**Table 8a.1** and **Figure 8a.3**). And also, for both approximately comparable frontier MO energy values were obtained for all the five occupied and unoccupied MO. In the case of both HOMO and LUMO, the exclusive MO contribution is delocalized in the attached indole ring of the NPT100-18A and NPT200-11. Furthermore, the corresponding nucleophilicity and electrophilicity indices (N and ω respectively) values were also evaluated to probe their affinity in response to the nearby environment. N and ω values can be estimated using equations $N = E_{HOMO} - E_{HOMO\ (TCNE)}$ (considering tetracyanoethylene (TCNE) as the

reference) [514] and $\omega = \mu^2/2\eta$ where $\mu = (E_{HOMO} + E_{LUME})/2$ and $\eta = (E_{HOMO} - E_{LUMO})$ [515-517] respectively. The calculated *N* and ω for NPT100-18A and NPT200-11 are listed in **Table 8a.2**. As in agreement with the HOMO and LUMO energies, both NPT100-18A and NPT200-11 also possessed comparable *N* and ω values. Also, the electron donation and acceptance ability of a compound in response to the environment can be probed by evaluating the properties of HOMO-LUMO band gap, ionization potential, electron affinity and electronegativity values (**Table 8a.2**). The adiabatic ionization potential and electron affinity of a system can be calculated by subtracting the energy values from their neutral closed-shell ones to the corresponding cationic and anionic species respectively. Interestingly, it is worth mentioning that these compounds may be considered strong reducing agent based on the values of their low ionization energies which is approximately comparable to the first ionization potential of lithium (124.3 kcal/mol). Both NPT100-18A and NPT200-11 possess a large comparable MO band gap, which essentially may predict their possible level of stability.

Table 8a.1. *Energies (in eV) of the first five highest occupied (HOMO, HOMO-1, HOMO-2, HOMO-3, and HOMO-4) and lowest unoccupied (LUMO, LUMO+1, LUMO+2, LUMO+3 and LUMO+4) frontier MO of NPT100-18A and NPT200-11 respectively in B3LYP+D3/def2-TZVP (/CPCM) level of theory*

Molecules	HOMO	HOMO-1	HOMO-2	HOMO-3	HOMO-4
NPT100-18A	-5.80	-6.11	-6.38	-6.78	-700
NPT200-11	-5.84	-6.30	-6.31	-6.79	-6.94
	LUMO	LUMO+1	LUMO+2	LUMO+3	LUMO+4
NPT100-18A	-0.75	-0.23	-0.14	0.08	0.24
NPT200-11	-0.71	-0.33	-0.04	0.08	0.26

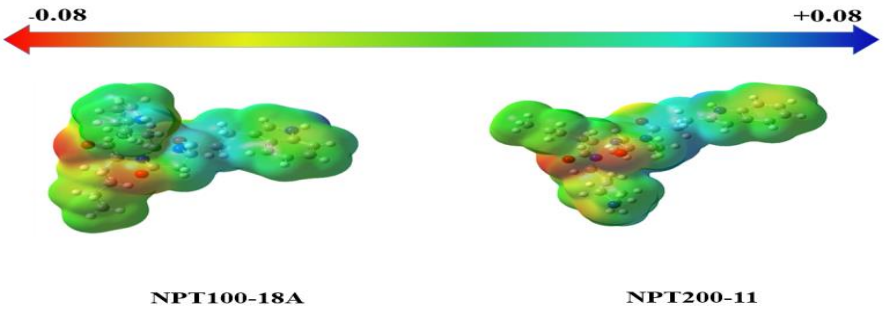

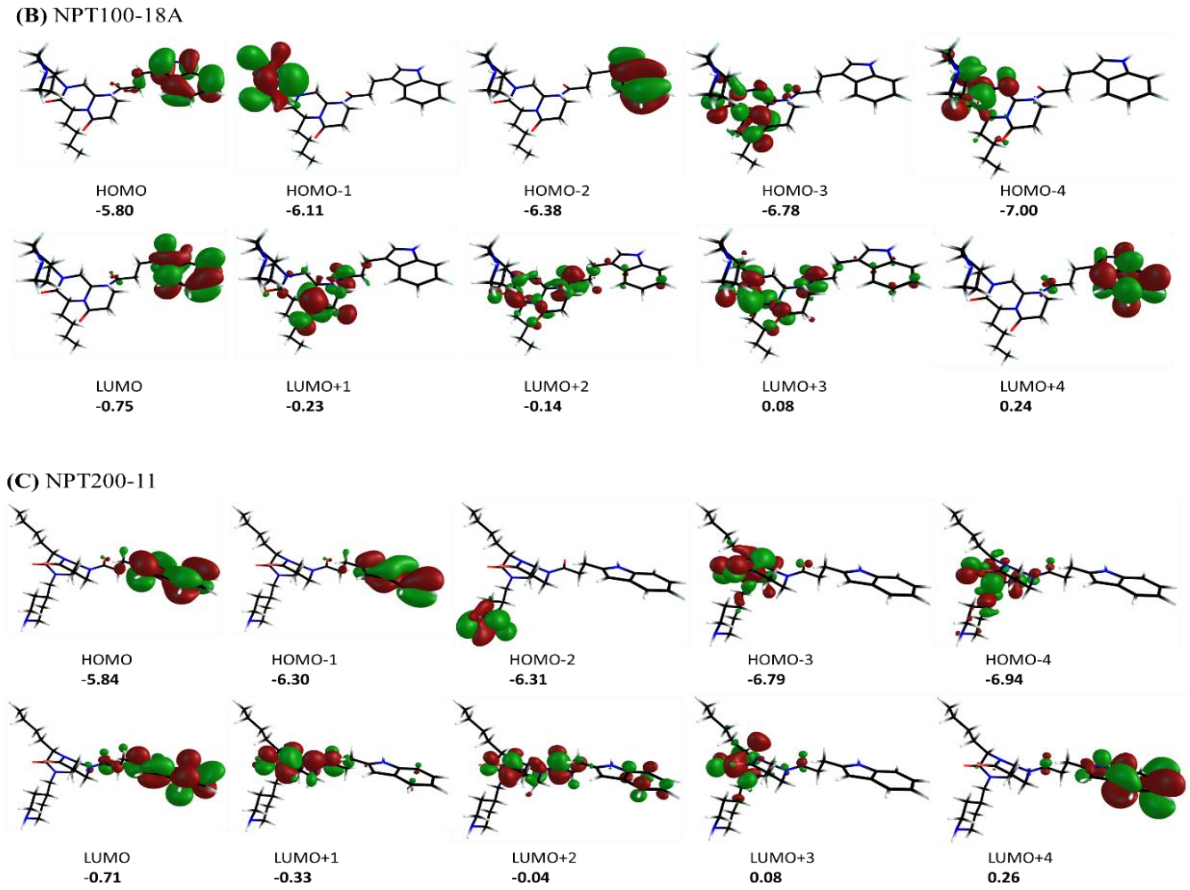

Figure 8a.3. *(A) Electron density plot of B3LYP+D3/def2-TZVP (/CPCM) calculated inhibitors (NPT100-18A and NPT200-11) according to the electrostatic potential map (ESP). Electrostatic potential energy data is estimated as a color spectrum, with red as the lowest electrostatic negative charge and blue as the highest to convey the varying intensities of the electrostatic potential maps. (B) and (C) represent the energies (in eV) of first five highest occupied (HOMO, HOMO-1, HOMO-2, HOMO-3, and HOMO-4) and lowest unoccupied (LUMO, LUMO+1, LUMO+2, LUMO+3 and LUMO+4) frontier MO of NPT100-18A and NPT200-11 respectively in B3LYP+D3/def2-TZVP (/CPCM) level of theory*

Table 8a.2. *Calculated values of nucleophilicity (N, eV) and electrophilicity (**ω,** eV) indices, ionization potential (IP, in kcal/mol), electron affinity (EA, in kcal/mol) and HOMO-LUMO band gap ($\Delta E_{HOMO-LUMO}$, in kcal/mol) for NPT100-18A and NPT200-11*

Molecules	*N*	*ω*	IP	EA	$\Delta E_{HOMO-LUMO}$
NPT100-18A	3.90	1.06	127.4	30.5	-116.5
NPT200-11	3.86	1.04	128.1	29.9	-118.3

To determine if the adopted simulation protocol is correct, lipid profile analyses such as Area per lipid analysis, membrane thickness analysis, and electron density profile analysis were carried out using MD trajectory files.

8a.4.2. Area per Lipid Analysis:

The density of a biomembrane is calculated by dividing its surface area by the number of lipids in the system. The average area per lipid surface (APL) was calculated as a criterion for determining equilibrium configurations in the DOPE/DOPS/DOPC simulation system. A value for the area per lipid layer was calculated by dividing the whole surface area of the simulation box by the total number of lipids in a single leaflet. To calculate the surface area per lipid layer, the total surface area of the simulated box was divided by the total number of lipids in a single leaflet. The APL for the DOPE/DOPS/DOPC lipid bilayer as a function of time is depicted in **Figure 8a.4**. Area per lipid for the DOPE/DOPS/DOPC system was calculated for NPT100-18A complex, NPT200-11 complex and α-Syn to be 69.50 $Å^2$, 67.39 $Å^2$ and 67.78 $Å^2$ for the upper leaflet and 72.17 $Å^2$, 69.98 $Å^2$ and 69.54 $Å^2$ for the lower leaflet over a 100 ns trajectory.

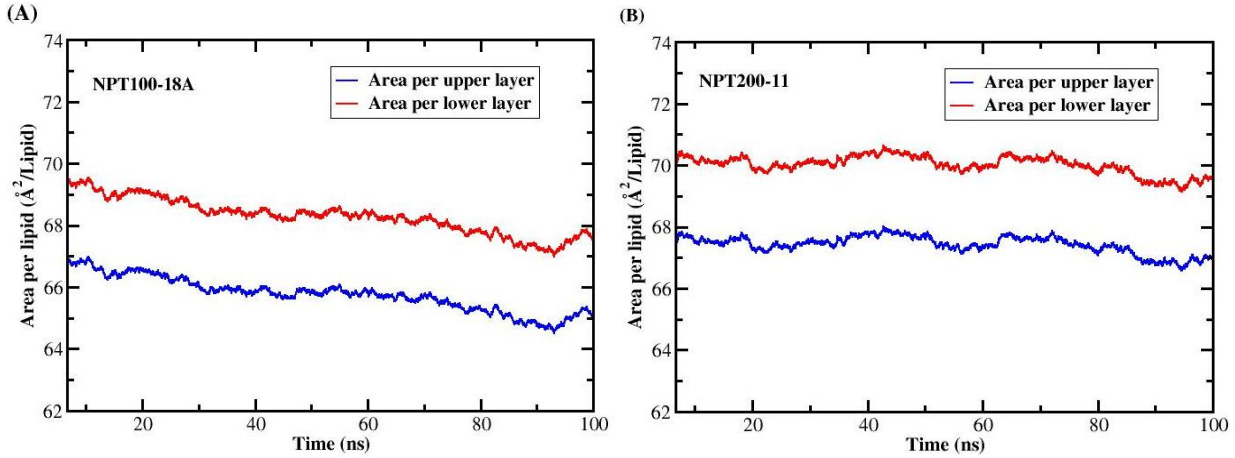

Figure 8a.4. *Area per lipid analysis for A) inhibitor NPT100-18A and (B) inhibitor NPT200-11 associated membrane bound α-Syn during MD simulation*

8a.4.3. Membrane Thickness analysis:

In addition, the average membrane thickness was determined by evaluating the distance that is the shortest between a phosphorus atom in one leaflet of a lipid layer and every phosphorus atom in the other leaflet of the lipid layer. This distance was used to calculate the average membrane thickness [459, 460, 23]. In **Figure 8a.5**, the membrane thickness plot shows the time evolution of the membrane thickness for DOPE/DOPS/DOPC mixed lipid bilayers, which are stable for a simulated time of 100 ns. The average membrane thickness was calculated to be 88.48 Å, 89.03 Å and 87.16 Å for the NPT100-18A complex, NPT200-11 complex and α-Syn respectively.

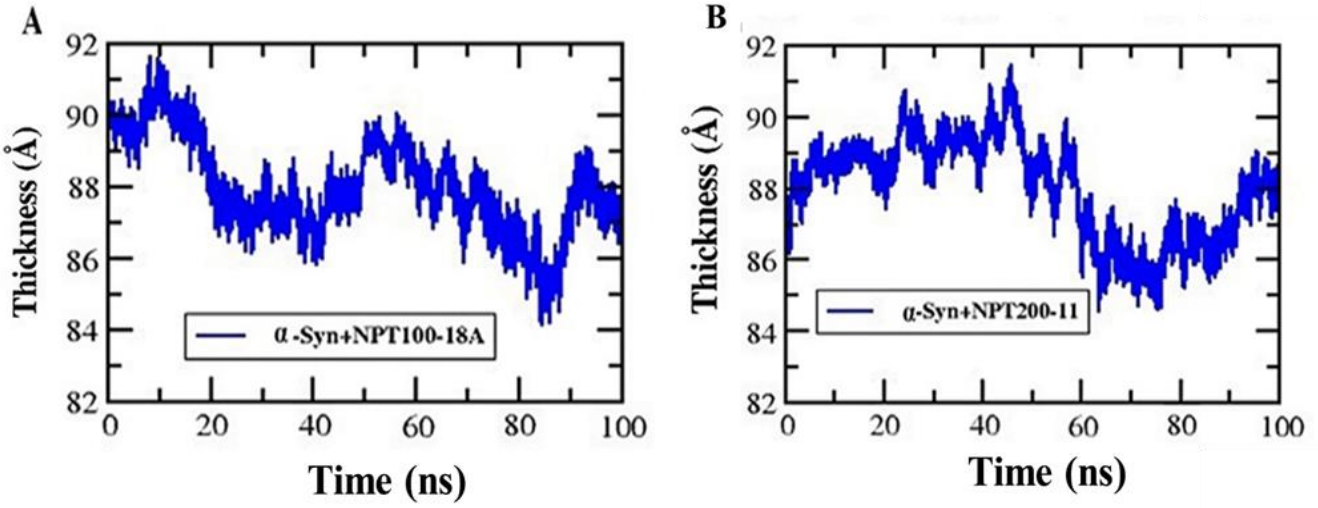

***Figure 8a.5**. Membrane thickness analysis of for (A) inhibitor NPT100-18A and (B) inhibitor NPT200-11 associated membrane bound α-Syn during MD simulation*

8a.4.4. Electron Density Profile Analysis:

To determine the Electron density profile (EDP), it was assumed that the central electron charge of each atom was equal to the atomic number minus the atomic partial charge. In the case of all-atom densities, three unique zones are seen in the density profiles of DOPE, DOPS, and DOPC. The lipid bilayer composed of DOPE, DOPS, and DOPC assembled in a 5:3:2 ratio on both lipid monolayers, defining the mixed lipid bilayer. The positioning of molecules and their chemical components within a lipid bilayer is frequently described using electron density profiles, as shown in **Figure 8a.6**. The EDP of different regions of α-Syn and in complex states (NPT100-18A and NPT200-11) is shown in **Figure 8a.7**. It is found that the N-helix region of both the α-Syn and complexes is buried immediately below the lipid head group/water interface, allowing the hydrophobic face of the protein to interact with the lipid membrane hydrophobic core and the hydrophilic face to connect with the lipid's polar region and water. The NPT100-18A complex buries 2 Å deeper than the NPT200-11 complex beneath the lipid head group phosphates. The N-helix of α-Syn tends to lie below the bilayer centre at a distance of 25 Å. In all the cases, Helix-N finishes up deeper than in the turn area, beneath the lipid head group phosphates. The average depth of the helix-C of α-Syn and NPT100-18A complex is below the bilayer centre (Z=0) at around 8 Å except for the NPT200-11 complex, which lies at a depth of 5 Å. The binding environment of membrane-bound α-Syn shows significant changes in the presence of NPT100-18A and NPT200-11 inhibitors compared to α-Syn. To expose some of itself to the water, the protein appears to occasionally tunnel through the bilayer. The two

peditomimetic inhibitors (NPT100-18A and NPT200-11) have been found mainly embedded in the major region of DOPE/DOPS/DOPC (phosphate group, ethanolamine, choline, serine, oleoyl group and water) lipid bilayer as shown in the Density plots (**Figure 8a.8**). Also noticed a shallower distribution of NPT100-18A inhibitor molecules (-20 Å to 20 Å) in the membrane that indicates an orientation of the molecules parallel to the membrane surface. In contrast, the distribution of the NPT200-11 inhibitor molecule was found to be relatively deeper (-30 Å to 35 Å) into the membrane. The interaction between two peptidomimetic inhibitors (NPT100-18A and NPT200-11) and membrane bilayer were depicted in the form of 3-D diagram in **Figure 8a.9** and **Figure 8a.10.** And the types of interactions (hydrogen bond and hydrophobic) between the two peptidomimetic inhibitors (NPT100-18A and NPT200-11) and membrane bilayer were obtained using Ligplot+ [254] as shown in **Figure 8a.11** and **Figure 8a.12** respectively**.** In Ligplot analysis of NPT100-18A and membrane bilayer (**Figure 8a.11**), the interactions were identified to be pe151, ps157, ps142, pe217, ol143, ol146, ol172, pe172, ol275, ol164, ol141, ol218. Similarly, for NPT200-11 and membrane bilayer, the ligplot analysis (**Figure 8a.12**) were identified to be ol243, ol141, ol146, pe145, ps142, ol1820, ol143, ol171, ps157.

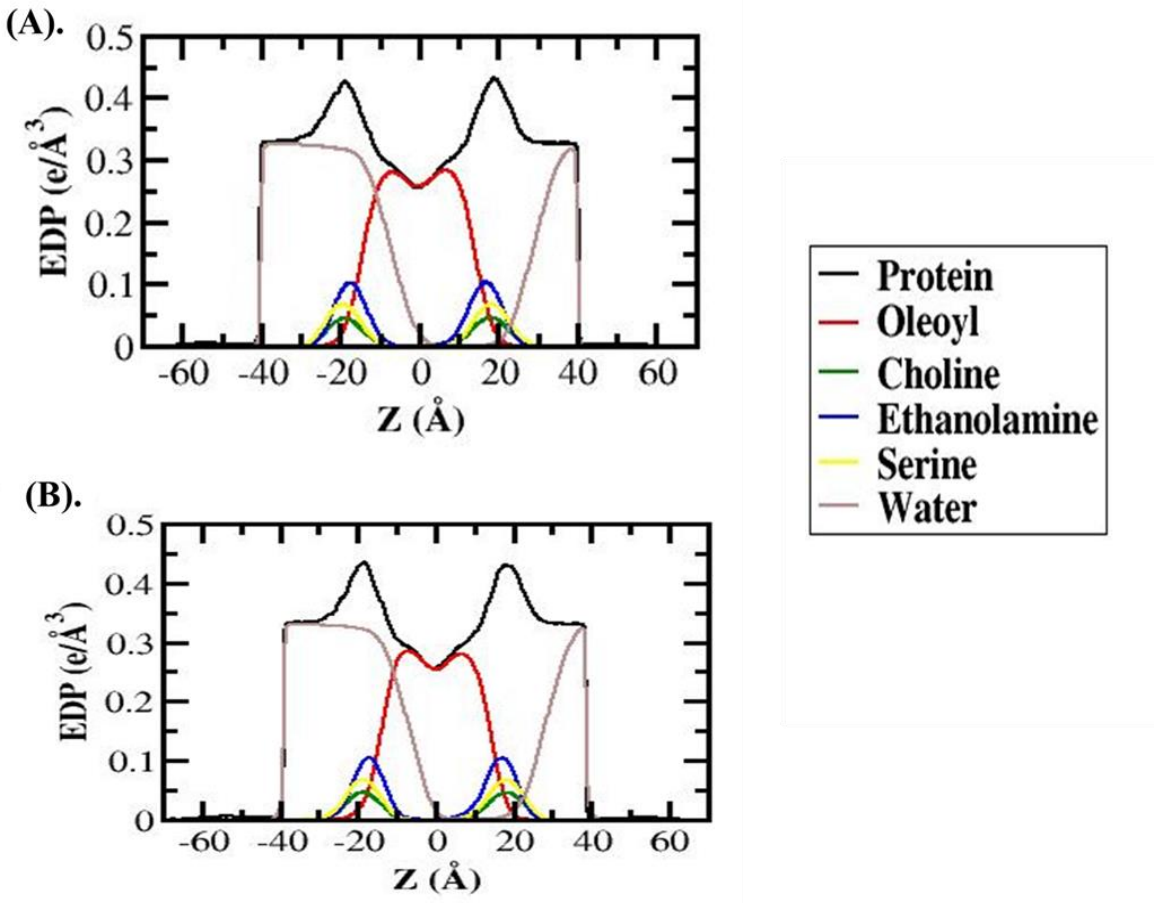

Figure 8a.6. *Electron density profile of (A) inhibitor NPT100-18A and (B) inhibitor NPT200-11 inhibitor attached to the α-Syn after the simulation*

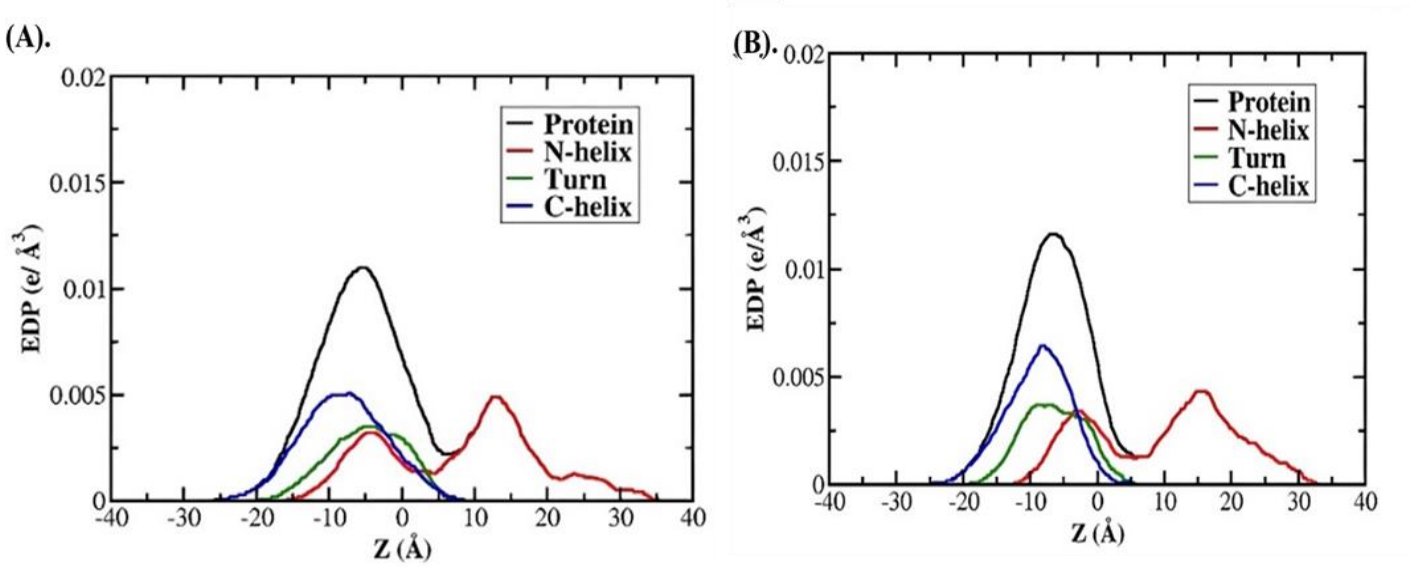

Figure 8a.7. *Electron density profile of (A) inhibitor NPT100-18A and (B) inhibitor NPT200-11 complexes after the simulation of 100 ns*

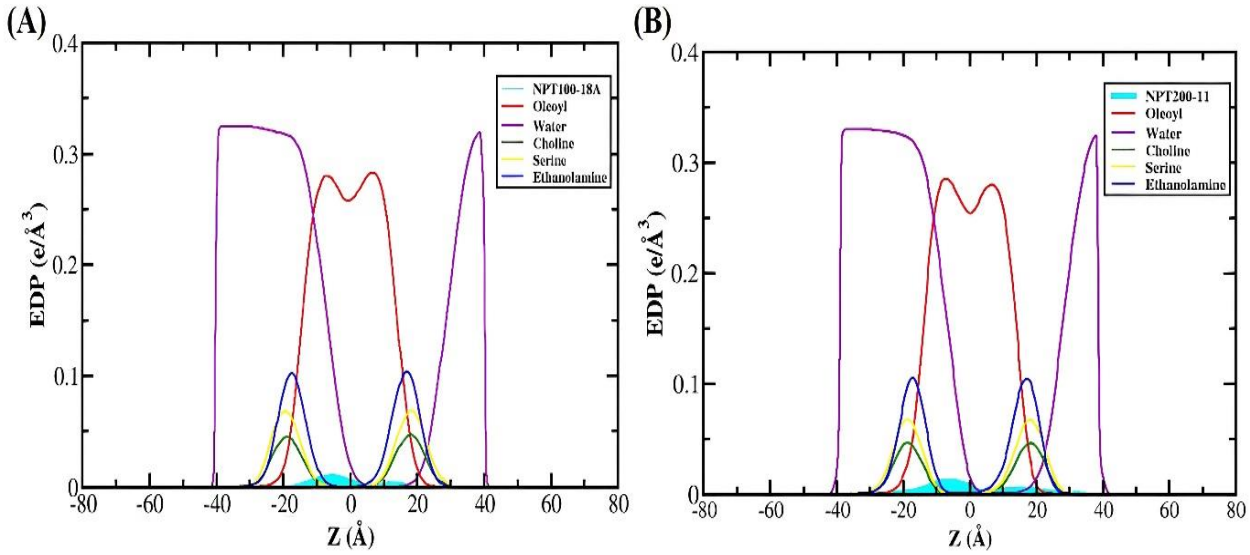

Figure 8a.8. *Electron density profile of (A) inhibitor NPT100-18A (B) inhibitor NPT200-11 in association with membrane bilayer after the simulation of 100 ns*

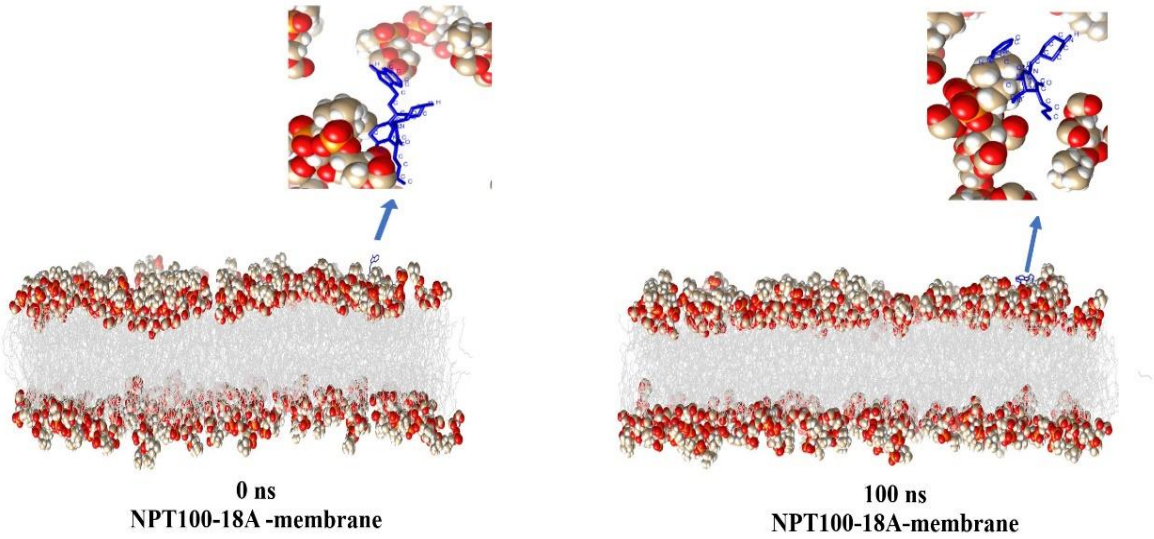

Figure 8a.9. *3-D snapshot of membrane bound α-Syn in presence of inhibitor NPT100-18A during MD simulation*

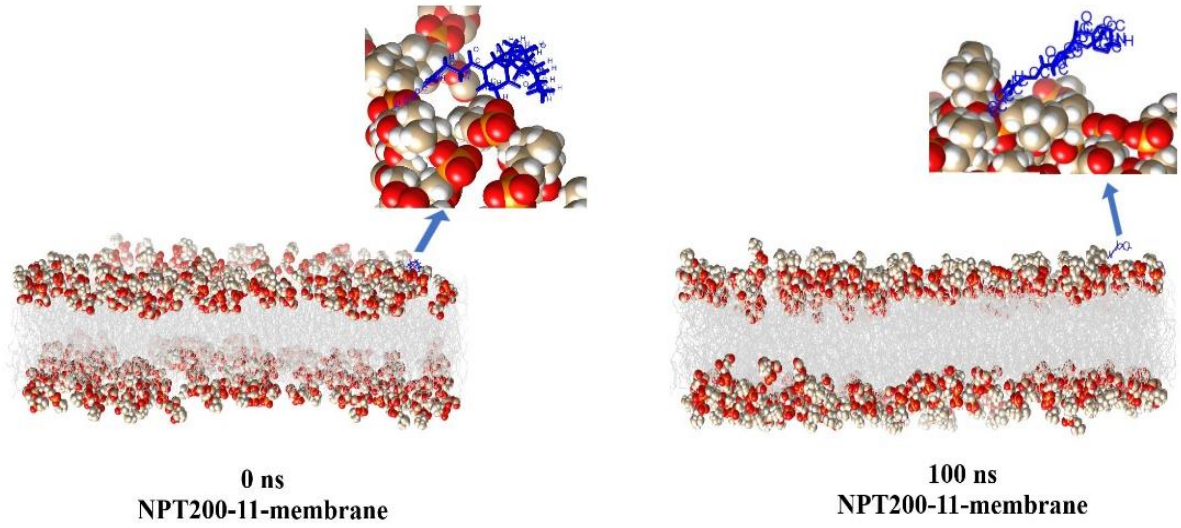

Figure 8a.10. *3-D snapshot of membrane bound α-Syn in presence of inhibitor NPT200-11 during MD simulation*

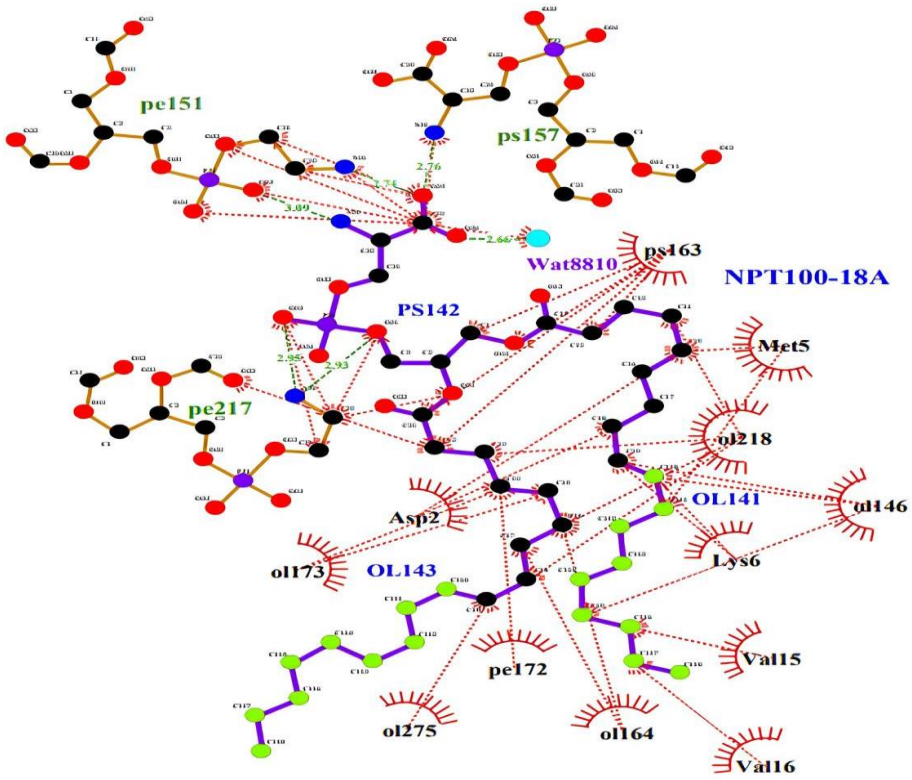

Figure 8a.11. *Ligplot analysis showing the interactions between NPT100-18A inhibitor and membrane bilayer during MD simulation*

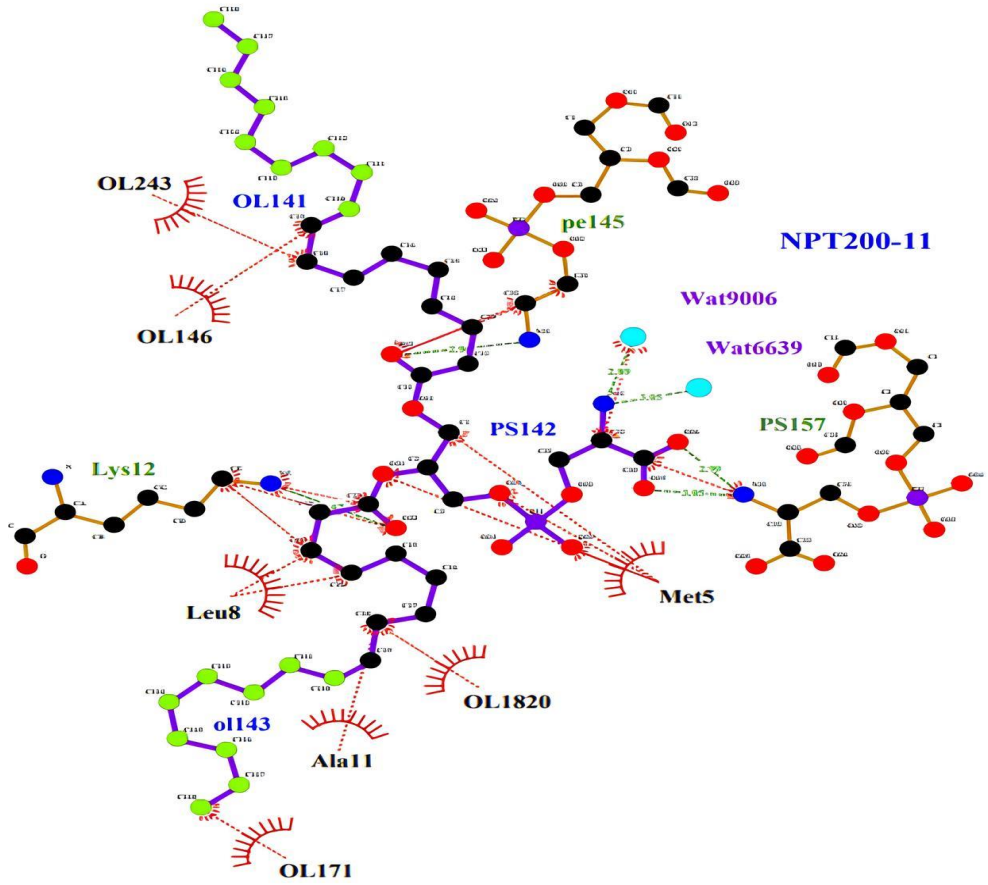

Figure 8a.12. *Ligplot analysis showing the interactions between NPT200-11 inhibitor and membrane bilayer during MD simulation*

8a.4.5. Conformational changes of docked membrane bound α-Synuclein and inhibitor molecule (NPT100-18A and NPT200-11) complexes during MD simulation:

The conformational dynamics of the 3-D structure of α-Syn in the presence of two peptidomimetic inhibitors (α-Syn-NPT100-18A, α-Syn-NPT200-11) have been shown in **Figure 8a.13** and **Figure 8a.14**. The snapshots have been taken at different intervals of simulation time. From **Figure 4.11**, the NAC region of WT α-Syn in apo state was observed to get elevated above the membrane surface and also observed the helix to be broken near the region 45–95. While in the presence of inhibitors, it was noticed that the helices to be retained in the regions 1-37 and 45-95, and also the α-Syn is bound firmly to the membrane, as shown in **Figure 8a.15**. Similar results have been reported in earlier studies [14, 25]. The α-helix can undergo an interconversion between two different conformations: an "extended helix," in which the regions (1-37) form a single helix that interacts with the lipid bilayer, and a "broken helix," in which the helix is broken at around the 45–95 position. In the bulk water phase, the α-Syn nucleus formed on the membrane attracts lipid-unbound monomers, which elongate to form long, unbranched amyloid fibrils along with a cross β-sheet structure. In the presence of an inhibitor, the overall structure of α-Syn is embedded into the lipid membrane, retaining the helical portion, thereby facilitating α-Syn conformers not suitable for aggregation. This agrees with the findings observed in our earlier study [518] that reported the effect of oleuropein aglycone, a standard inhibitor molecule for α-Syn aggregation. In the presence of oleuropein aglycone, it was observed that the α-Syn contains higher helical content and promotes the development of non-toxic aggregates.

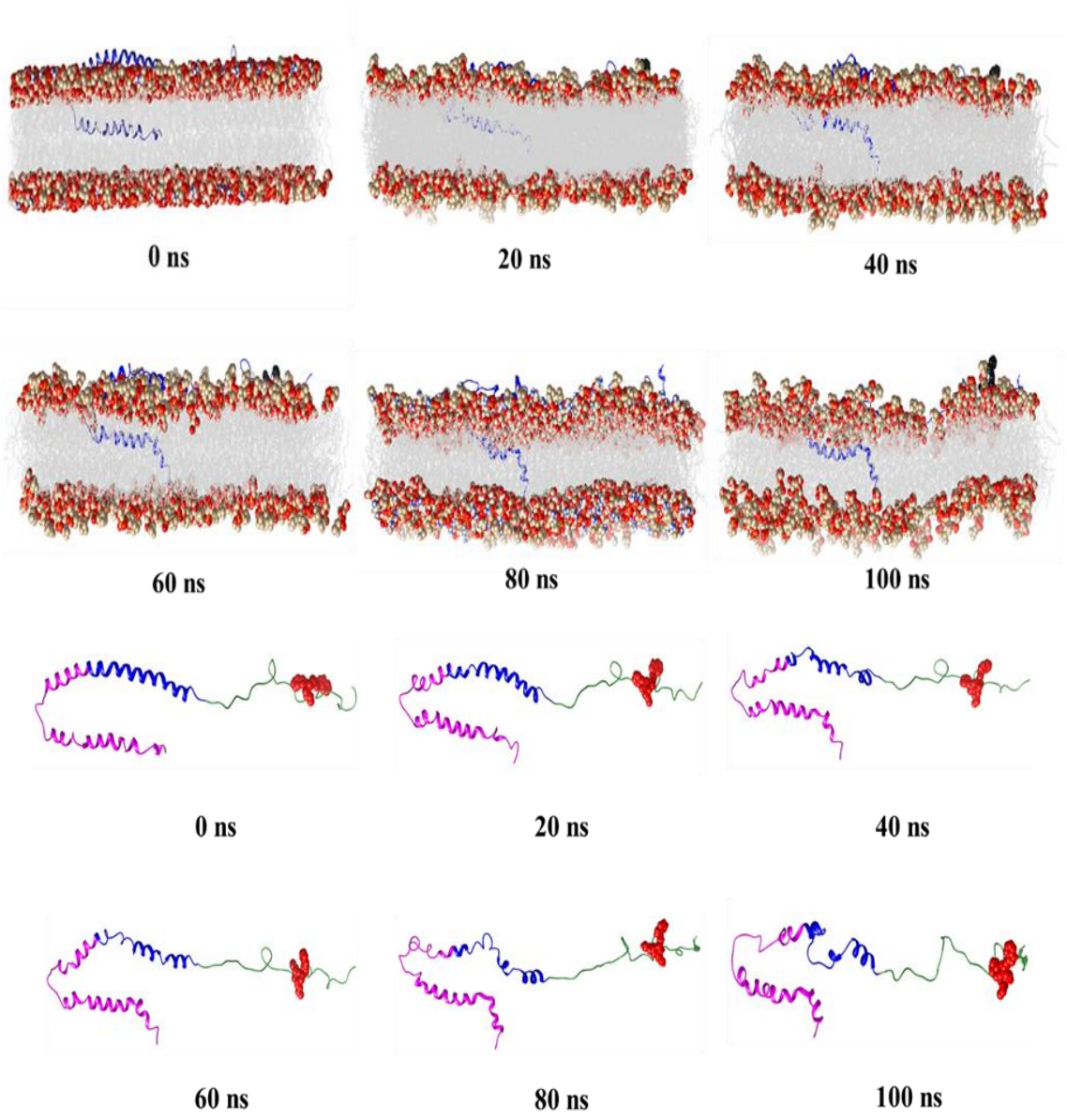

Figure 8a.13. *Snapshots of conformational changes observed in membrane bound α-Syn in presence NPT100-18A inhibitor*

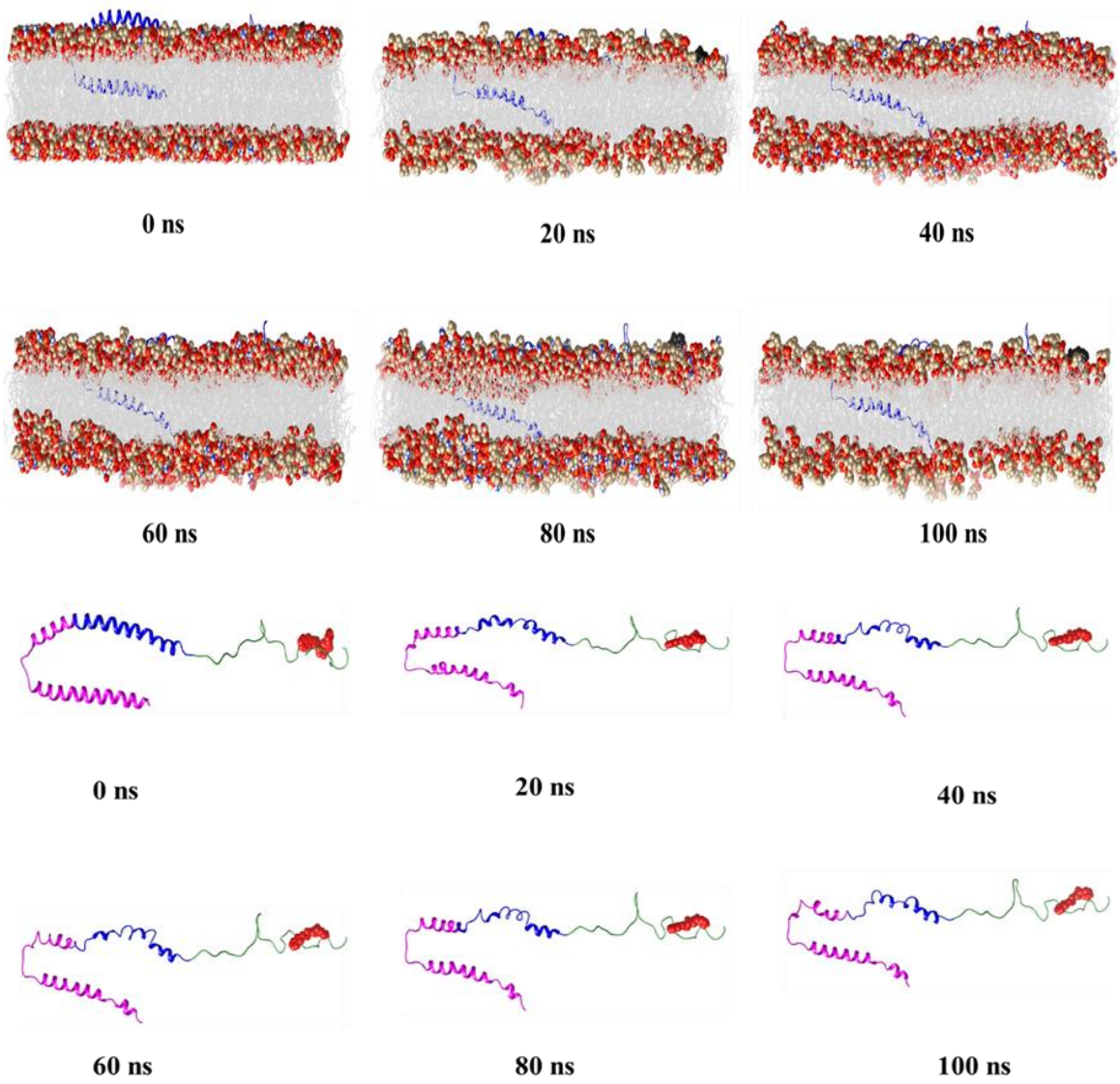

Figure 8a.14. *Snapshots of conformational changes observed in membrane bound α-Syn in presence NPT200-11 inhibitor*

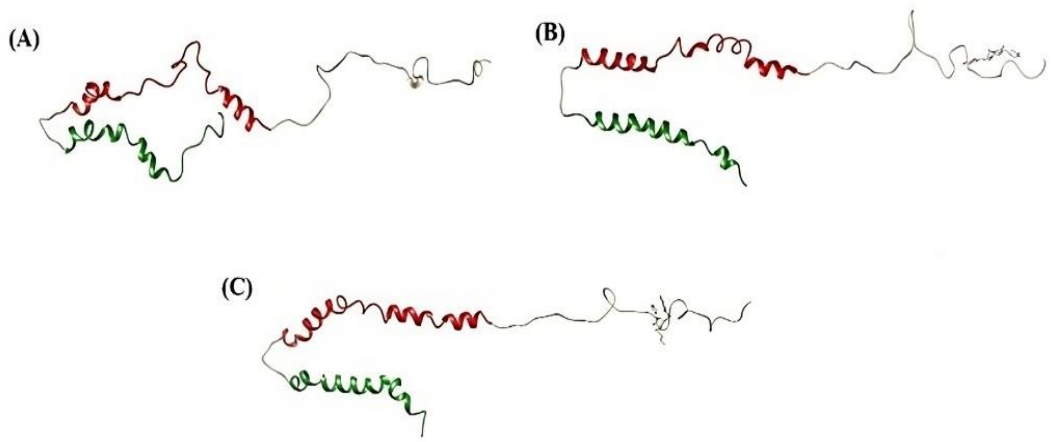

Figure 8a.15. *Snapshots of (A) α-Syn (B) α-Syn+NPT100-18A and (C) α-Syn+NPT200-11 showing N-terminal (residue 1-37) in green color and NAC region (residues 45-95) in red color after MD simulation run of 100 ns*

8a.4.6. RMSD Analysis:

The RMSD analysis of Cα atom of each component of α-Syn and inhibitor (NPT100-18A and NPT200-11) complexes during the simulation time were depicted in **Figure 8a.16 (A)**. The overall structure of α-Syn was observed to adopt stable conformational dynamics in the presence of inhibitors rather than in the WT α-Syn in the apo state as observed in section **4.4.4.** But the NAC region in the α-Syn showed subtle changes in the conformation, as shown in **Figure 8a.17**. From **Figure 8a.16 (B)**, it can be seen that the two peptidomimetic inhibitors adopt rigid conformational dynamics as they have been bound strongly to the C-terminal region of α-Syn.

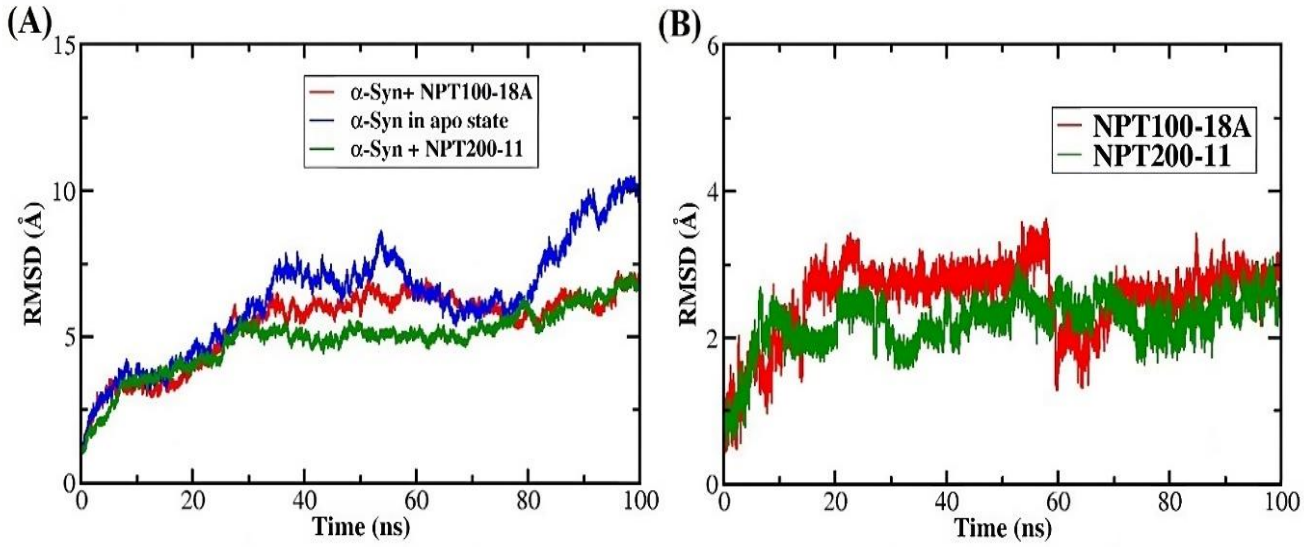

Figure 8a.16. *RMSD analysis of (A) α-Syn and inhibitor (NPT100-18A and NPT200-11) α-Syn complexes (B) RMSD analysis of inhibitors (NPT100-18 and NPT200-11) after the simulation of 100 ns*

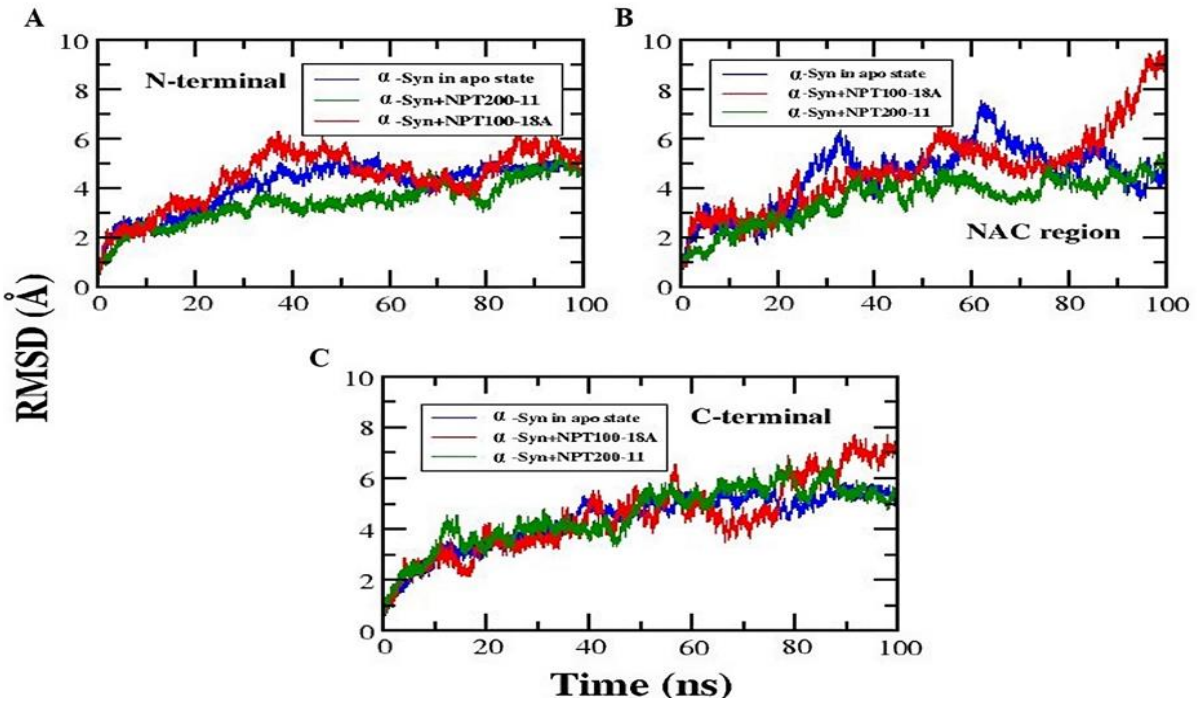

Figure 8a.17. *RMSD analysis of (A) N-terminal (B) NAC region and (C) C-terminal of α-Syn apo and inhibitor (NPT100-18A and NPT200-11) complexes*

8a.4.7. Principal Component Analysis (PCA) followed by free energy landscape analysis:

PCA and free energy landscapes were used to evaluate simulated structures of α-Syn in the presence of the inhibitors. The MD trajectory information of the Cα atoms (after the systems have reached stabilisation) was used for the PCA. The first few major components provide global and local mobility. In our work, two directional principal components (PCs), defined as the first eigenvector (PC1) and the second eigenvector (PC2), contribute to protein global motion. PC1 and PC2 generated 2D and 3D free energy landscapes to visualise the protein systems' sampling space (as shown in **Figure 8a.18**). From the **Figure 4.7** of the section **4.4.5**, eigenvalues of WT α-Syn in the apo state fluctuate more rapidly than in the presence of inhibitors as observed in the case of the RMSD plot (**Figure 8a.16**), demonstrating that binding of NPT200-11 and NPT100-18A to α-Syn creates a stable cluster and occupies the least phase space. It is noticed that all the systems were found to have one global minimum and one or two subsidiary minima. However, the energy difference between global minima and secondary minima were found to be of the order of 1.5 kcal/mol or less. Thus, simulated structures have one main conformation with considerable flexibility [303, 304].

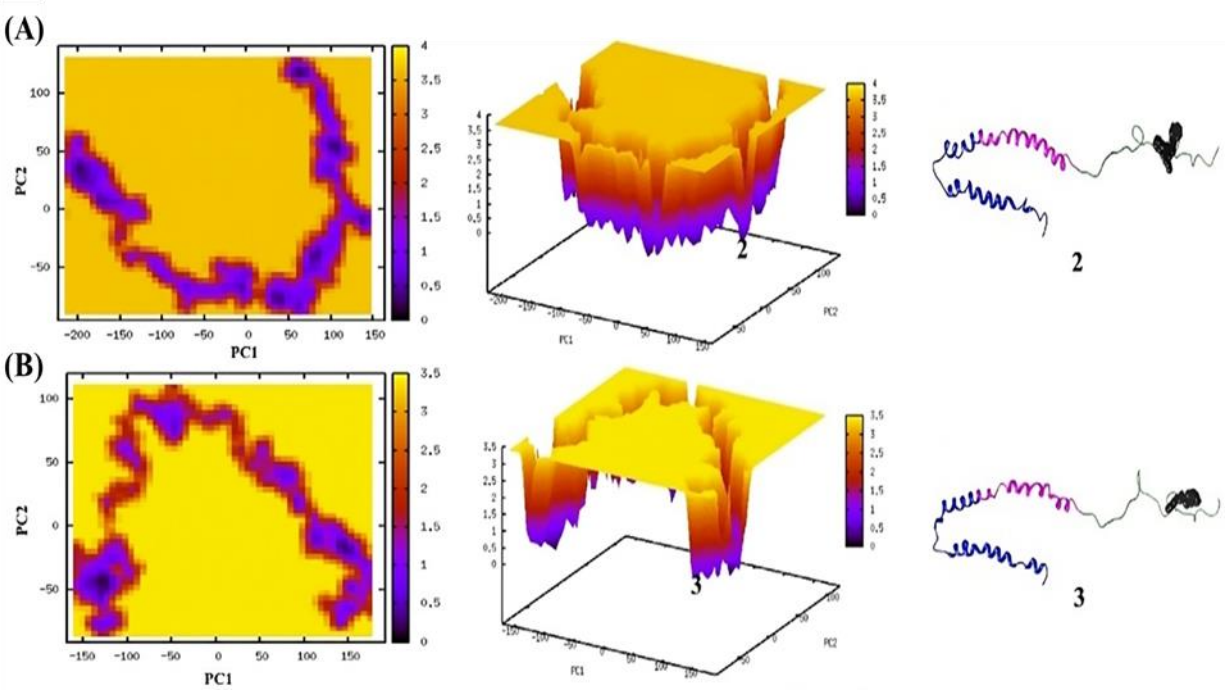

Figure 8a.18. *PCA followed by 2D (left) and 3D (middle) free energy landscapes (FEL) analysis of α-Syn in the presence of (A) inhibitors NPT100-18A and (B) NPT200-11 respectively. X, Y, and Z indicate PC1, PC2, and free energy, respectively. In the energy well, '2', and '3' reflect the global minimum of α-Syn in the presence (A and B) of inhibitors NPT100-18A and NPT200-11. Colour-coded mode was used to correlate structural conformations and free energy of α-Syn in the presence of inhibitors NPT100-18A and NPT200-11. The right-most panel shows energy wells with global free energy minima for α-Syn in the presence of inhibitors*

8a.4.8. RMSF Analysis:

To determine the flexible and rigid regions in the structure of α-Syn presence of peptidomimetic inhibitors (NPT200-11 and NPT100-18A), RMSF analysis with respect to the Cα atom has been carried out. The RMSF profile shown in **Figure 8a.19** dictates relatively higher flexibility in α-Syn when it is in free form as observed in section **4.4.6** than in the complex form with peptidomimetic inhibitors. The region near the NAC domain (40–70) in the α-Syn was observed to have higher flexibility.

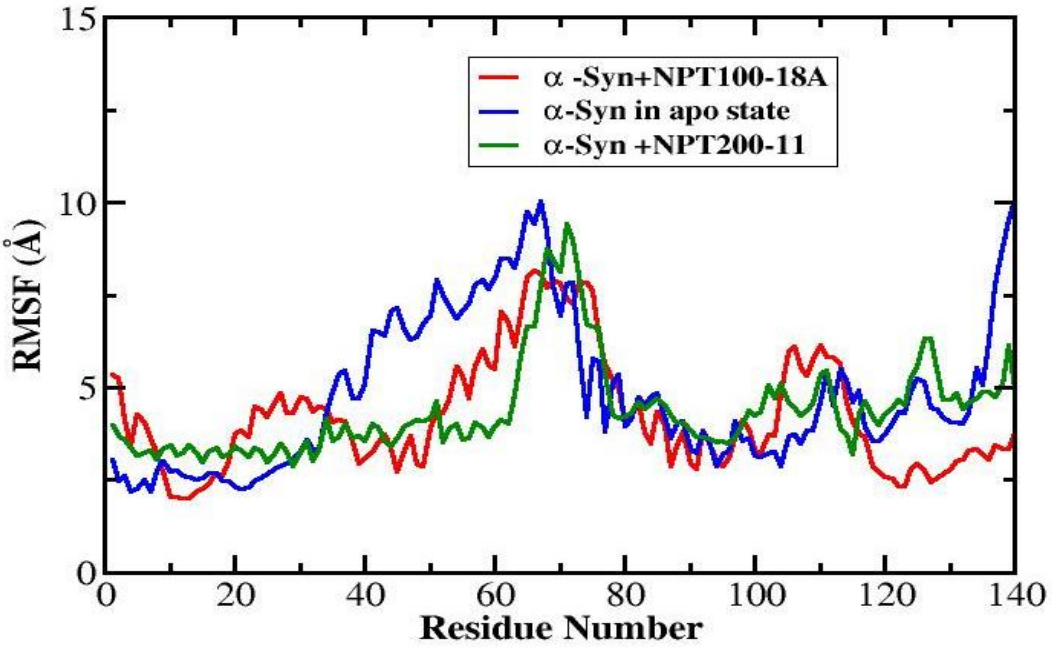

Figure 8a.19. *RMSF analysis of membrane-bound α-Syn and inhibitors (NPT100-18A and NPT200-11) - α-Syn complexes after the simulation of 100 ns*

8a.4.9. Distance Analysis:

The centre of mass distance between different domains of α-Syn has been determined in the presence of peptidomimetic inhibitors, as shown in **Figure 8a.20**. From **Figure 8a.20**, it was noticed that the centre of mass distance between different regions of α-Syn gets altered to a lesser extent in comparison with the distance between NAC and C terminal region. The centre of mass distance between the NAC region and C-terminal of WT α-Syn in the apo state showed elevation causing bending of the NAC region as mentioned in section **4.4.10**.

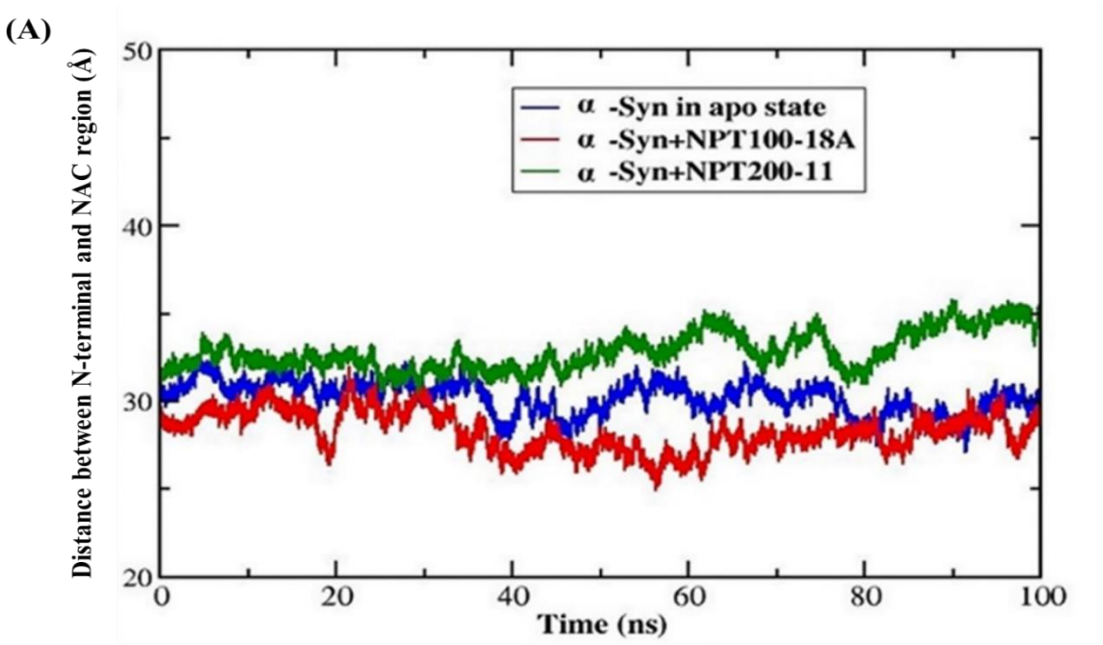

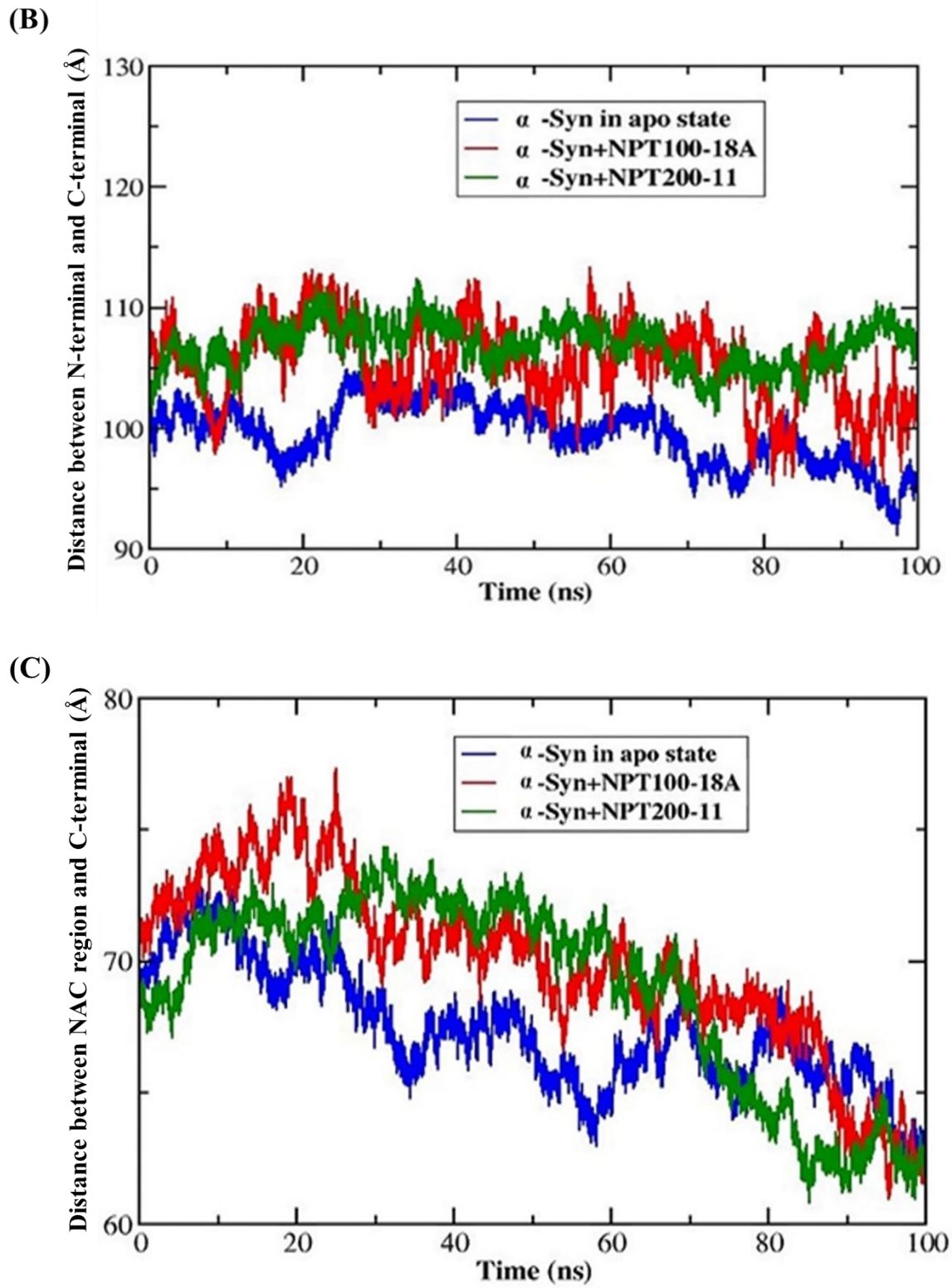

Figure 8a.20. *Distance analysis between (A) N-terminal and NAC region and (B) N-terminal and C-terminal and (C) NAC region and C-terminal of α-Syn in presence and absence of peptidomimetic inhibitors*

8a.4.10. Secondary Structural Analysis:

The time evolution of the secondary structure for the α-Syn in the presence of peptidomimetic inhibitors using the Kabsch and Sander algorithm [295] were depicted in **Figure 8a.21**. Secondary structural components, specifically α-helical content in the N-terminal and NAC regions of α-Syn were found to be relatively higher when it is in complex form with peptidomimetic inhibitors. The probable secondary structure with respect to residues of α-Syn has been shown in the plot **Figure 8a.22** and **Figure 8a.23**. The percentage α-helical content calculated for the well-equilibrated structure of α-Syn in the presence of inhibitors has been summarised in **Table 8a.3**. In the presence of inhibitors, the α-Syn was found to contain a higher helical content.

Table 8a.3. *Secondary structural content of the α-Syn in presence of inhibitors (NPT100-18A and NPT200-11) during MD simulation*

Complex	α-helix %	β-sheet %	turn %	Pi-helix %	3_{10} helix %	Coil %
NPT100-18A-α-Syn	24.6	0	21.4	0	7.5	46.4
NPT200-11-α-Syn	28.6	0	28.6	0	0	42.9

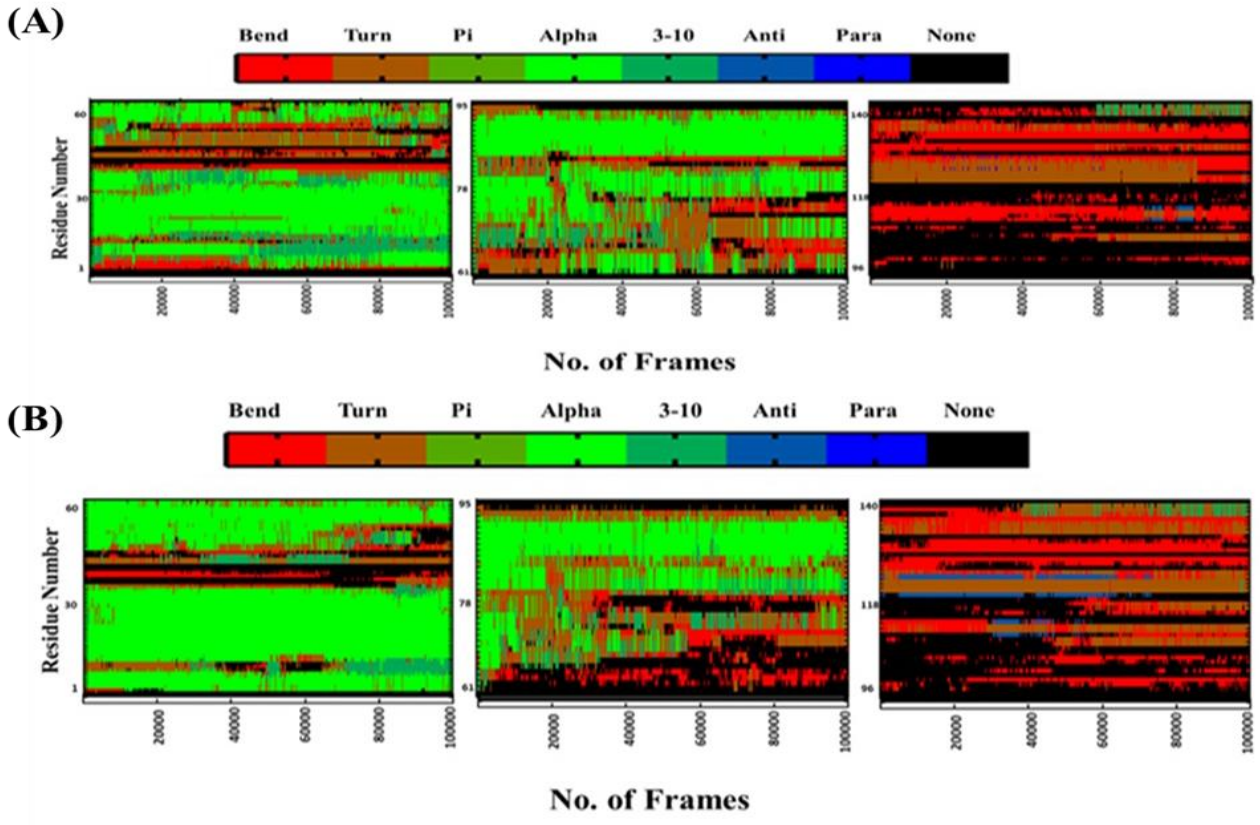

Figure 8a.21. *DSSP plot of secondary Structural content of α-Syn in the presence of inhibitor (A) NPT100-18A and (B) NPT200-11 complex during MD simulation obtained from Kabsch and Sander algorithm*

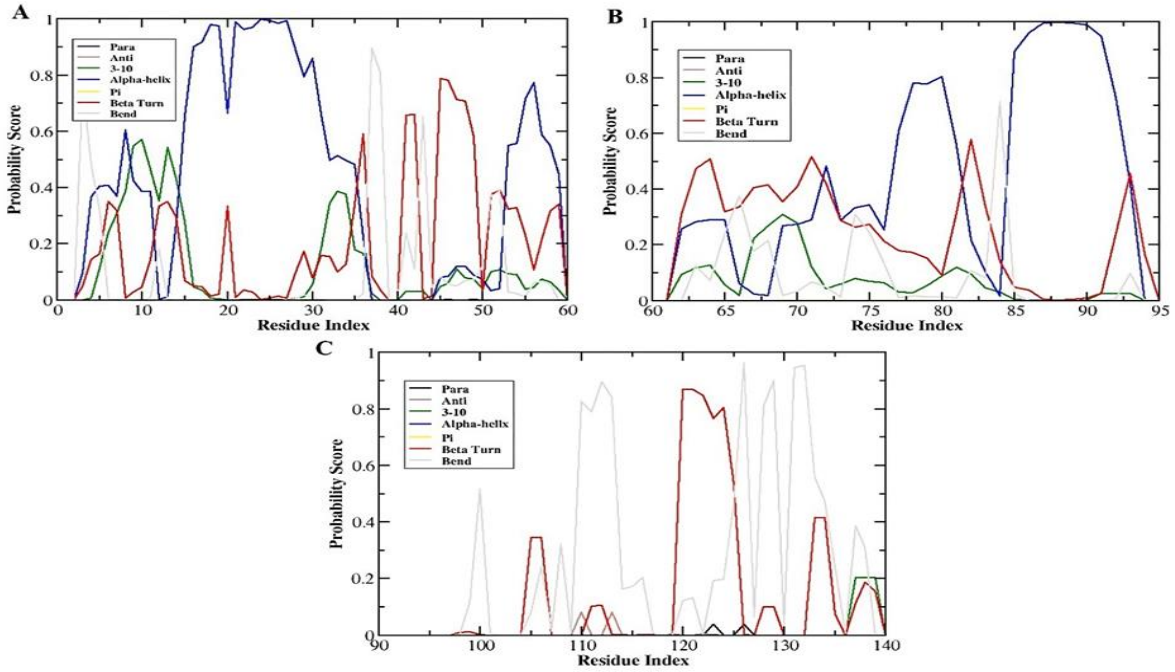

Figure 8a.22. *Secondary structure Probability score of (A) N-terminal (B) NAC region and (C) C-terminal of α-Syn in presence of NPT100-18A inhibitor*

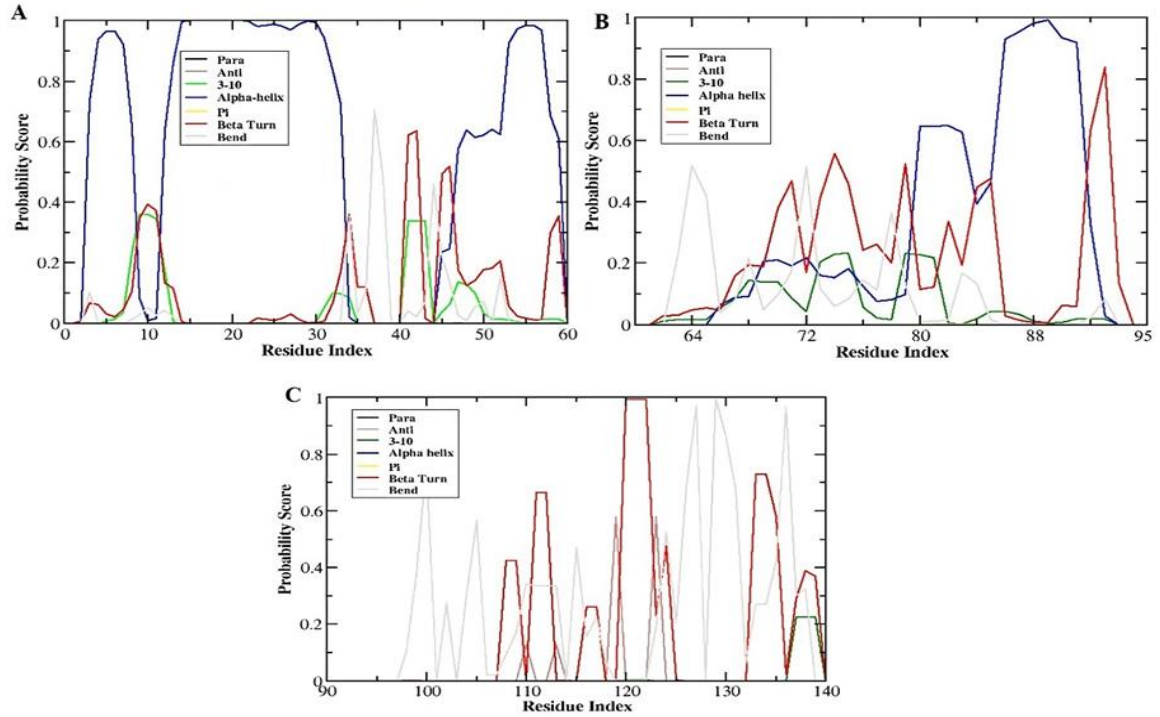

Figure 8a.23. *Secondary structure Probability score of (A) N-terminal (B) NAC region and (C) C-terminal of α-Syn in presence of NPT200-11 inhibitor*

8a.4.11. Intermolecular Hydrogen bond analysis:

To investigate the proximity between the lipid bilayer and different regions of α-Syn in the presence of inhibitors (NPT200-11 and NPT100-18A), the intermolecular hydrogen bond analysis was carried out as shown in **Figure 8a.24**. From **Figure 8a.24**, it was seen that when α-Syn is in complex form with peptidomimetic inhibitors, the number of intermolecular hydrogen bonds was relatively higher. Among the three different regions of α-Syn, the NAC region of α-Syn was found to have a lesser number of hydrophobic contacts with the membrane WT α-Syn in the apo state as observed in section **4.4.9**. The atomic-level details regarding the intermolecular hydrogen bonds between the lipid bilayer (acceptor/donor) and α-Syn (acceptor/donor) in the presence of peptidomimetic inhibitors were summarised in **Tables 8a.4-8a.7** respectively.

(A)

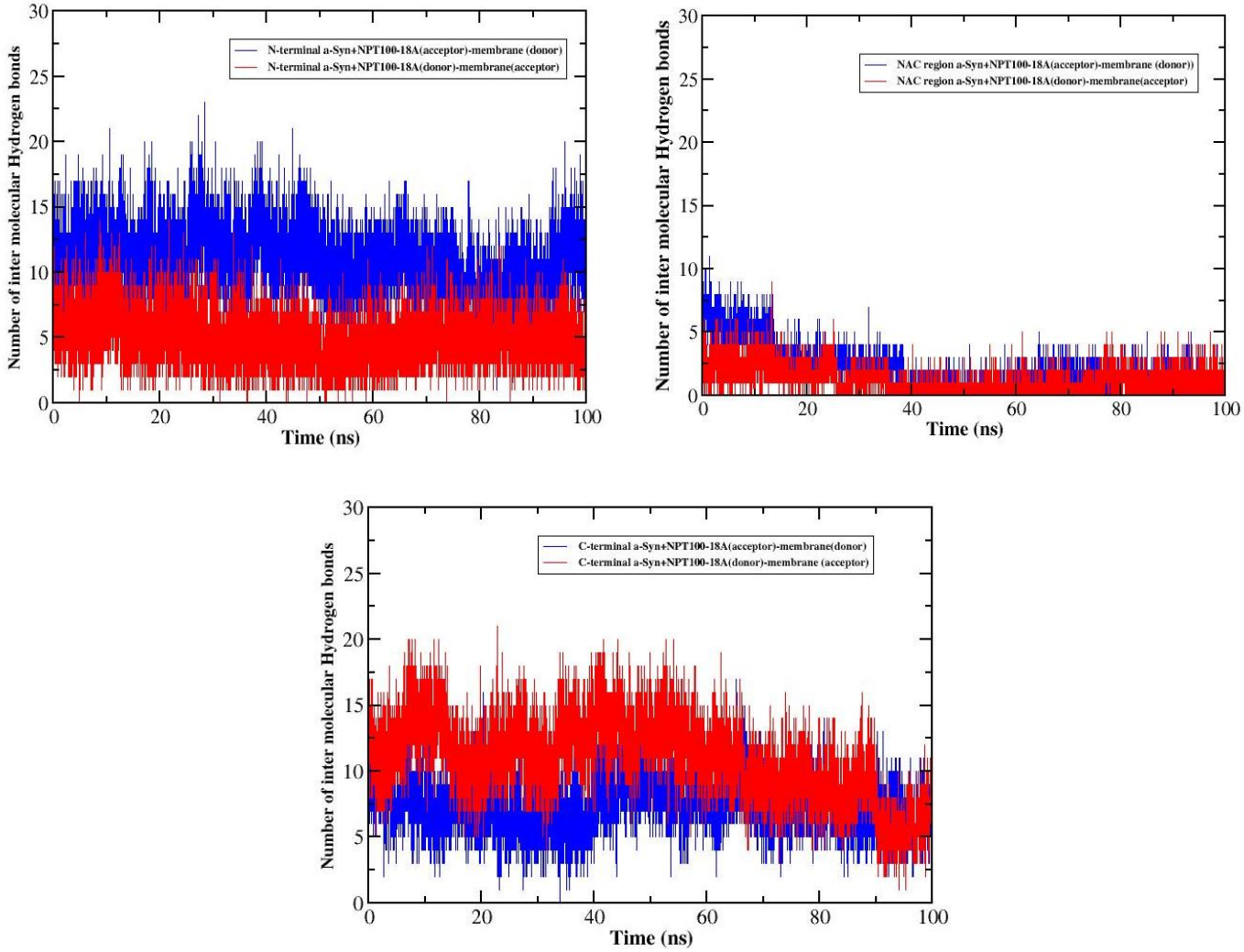

(B)

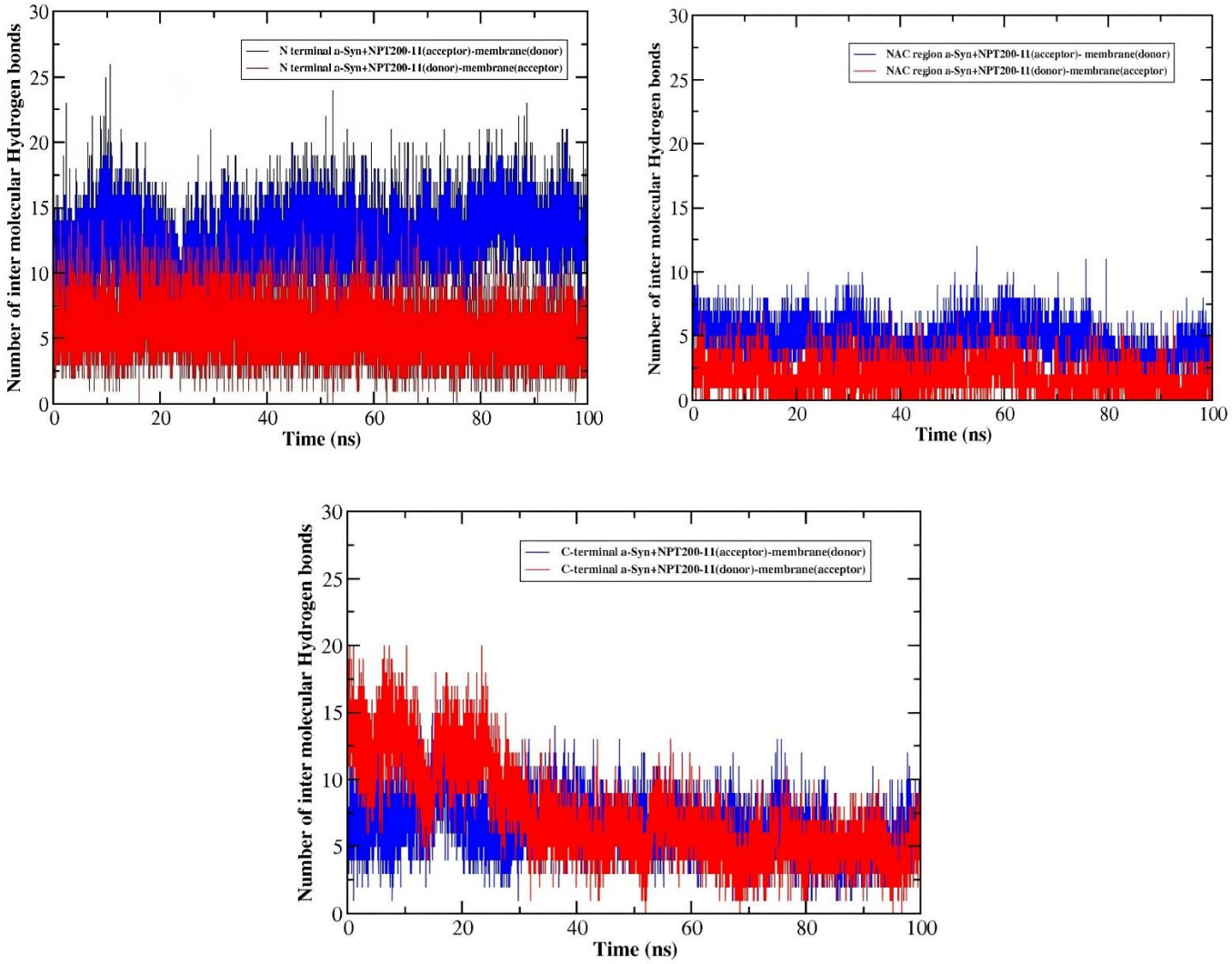

Figure 8a.24*. The number of intermolecular Hydrogen bond analysis between membrane bilayer and all the regions of (A) NPT100-18A and (B) NPT200-11 complexes*

Table 8a.4. *Intermolecular Hydrogen bond analysis of membrane bound NPT100-18A-α-Syn complex during the MD simulation of 100 ns with membrane bilayer as acceptor and α-Syn in presence of NPT100-18A inhibitor as donor*

#Acceptor	DonorH	Donor	Average Distance (Å)	Average Angle (º)
PE_1777@O22	TYR_133@HH	TYR_133@OH	2.6989	159.7186
PS_163@O33	ASP_2@H	ASP_2@N	2.825	157.9569
PE_1864@O33	TYR_39@HH	TYR_39@OH	2.6468	163.2248
PE_1777@O34	GLN_134@HE22	GLN_134@NE2	2.7804	161.6335
PS_1795@O22	ASN_103@HD22	ASN_103@ND2	2.8226	161.8685
PC_1828@O34	GLN_24@HE22	GLN_24@NE2	2.7766	152.408
PE_1900@O34	GLN_109@HE21	GLN_109@NE2	2.7883	153.6125
PS_1813@O34	LYS_97@HZ2	LYS_97@NZ	2.7447	156.0879

PS_1813@O22	LYS_97@HZ3	LYS_97@NZ	2.77	158.4608
PE_1843@O34	LYS_12@HZ3	LYS_12@NZ	2.7663	160.0153
PS_163@O33	MET_1@H3	MET_1@N	2.8003	156.3654
PS_1813@O34	LYS_97@HZ3	LYS_97@NZ	2.7421	156.7966
PE_1885@O33	LYS_10@HZ1	LYS_10@NZ	2.7585	158.6184
PS_1846@O33	LYS_80@HZ2	LYS_80@NZ	2.7332	161.4323
PE_1885@O33	LYS_10@HZ2	LYS_10@NZ	2.7497	158.2069
PE_1843@O33	LYS_80@HZ1	LYS_80@NZ	2.7313	159.6423
PS_163@O33	MET_1@H1	MET_1@N	2.8052	155.4935
PS_1813@O34	LYS_97@HZ1	LYS_97@NZ	2.7469	155.2488
PC_1762@O22	GLU_130@H	GLU_130@N	2.8637	145.3985
PE_1843@O34	LYS_12@HZ2	LYS_12@NZ	2.7619	159.6575
PS_163@O33	MET_1@H2	MET_1@N	2.797	155.7938
PE_1765@O34	LYS_102@HZ1	LYS_102@NZ	2.7413	159.4433
PE_1765@O34	LYS_102@HZ3	LYS_102@NZ	2.7506	158.1229
PE_1861@O33	SER_42@HG	SER_42@OG	2.6242	165.3596
PE_1843@O22	LYS_12@HZ2	LYS_12@NZ	2.7802	152.8055
PS_1813@O22	LYS_97@HZ1	LYS_97@NZ	2.769	156.7077
PS_1813@O22	LYS_97@HZ2	LYS_97@NZ	2.7723	157.9824
PC_1771@O22	TYR_39@HH	TYR_39@OH	2.6576	163.9117
PE_1765@O34	LYS_102@HZ2	LYS_102@NZ	2.7471	158.3965
PE_1834@O34	THR_81@HG1	THR_81@OG1	2.6286	165.6532
PE_1843@O33	LYS_80@HZ3	LYS_80@NZ	2.7102	159.1038
PE_1942@O22	LYS_12@HZ1	LYS_12@NZ	2.7595	152.3003
PC_1828@O33	LYS_21@HZ2	LYS_21@NZ	2.7573	158.1374
PS_1846@O33	LYS_80@HZ1	LYS_80@NZ	2.7164	160.7684
PC_1828@O33	LYS_21@HZ1	LYS_21@NZ	2.7612	158.957
PE_1942@O22	LYS_12@HZ2	LYS_12@NZ	2.7594	152.1764
PE_1861@O34	SER_42@HG	SER_42@OG	2.6346	164.7212
PS_163@O34	MET_1@H1	MET_1@N	2.7718	150.2629
PC_1828@O21	GLN_24@HE22	GLN_24@NE2	2.8773	151.388
PE_1786@O34	TYR_136@HH	TYR_136@OH	2.6651	163.9865
PS_142@O33	MET_1@H2	MET_1@N	2.762	153.039
PC_1828@O33	LYS_21@HZ3	LYS_21@NZ	2.7586	157.7666
PS_1795@O35	ASN_103@HD22	ASN_103@ND2	2.7962	161.1592
PS_1870@O12	GLU_137@H	GLU_137@N	2.8439	154.4916
PE_1885@O33	LYS_10@HZ3	LYS_10@NZ	2.7478	155.4635
PE_1843@O22	LYS_12@HZ1	LYS_12@NZ	2.7855	156.4922
PS_142@O33	MET_1@H1	MET_1@N	2.7601	153.2271
PC_1828@O33	GLN_62@HE21	GLN_62@NE2	2.7962	160.4602
PS_1837@O22	SER_42@HG	SER_42@OG	2.6832	163.0707
PE_1900@H2A	ASP_115@HB3	ASP_115@CB	2.9027	152.1444

Table 8a.5. *Intermolecular Hydrogen bond analysis of membrane bound NPT100-18A-α-Syn complex complex during the MD simulation of 100 ns with α-Syn in presence of NPT100-18A inhibitor as acceptor and membrane bilayer as donor*

#Acceptor	DonorH	Donor	Average Distance (Å)	Average Angle (º)
ASP_115@OD1	PE_1852@HN1A	PE_1852@N31	2.7758	157.5068
GLU_110@OE1	PE_1903@HN1C	PE_1903@N31	2.7822	155.6987
ASP_115@OD2	PE_1903@HN1B	PE_1903@N31	2.7571	159.8271
GLU_110@OE1	PE_1852@HN1B	PE_1852@N31	2.7838	155.3572
GLU_131@OE2	PE_1858@HN1A	PE_1858@N31	2.7899	157.3452
GLU_28@OE1	PE_1855@HN1C	PE_1855@N31	2.7944	154.4087
GLU_28@OE1	PE_1855@HN1B	PE_1855@N31	2.7919	154.8074
GLU_131@OE1	PE_1858@HN1A	PE_1858@N31	2.7903	155.7109
GLU_28@OE2	PE_1855@HN1C	PE_1855@N31	2.8052	152.4831
GLU_105@OE2	PE_1765@HN1C	PE_1765@N31	2.7993	153.037
ASP_115@OD2	PE_1903@HN1C	PE_1903@N31	2.7607	158.1701
GLU_137@OE2	PE_1807@HN1A	PE_1807@N31	2.778	157.0242
GLU_28@OE2	PE_1855@HN1A	PE_1855@N31	2.7814	156.626
GLU_104@OE1	PS_1795@HN1C	PS_1795@N31	2.7888	158.0318
GLU_105@OE1	PE_1765@HN1C	PE_1765@N31	2.8067	153.2439
ASP_135@OD2	PE_1786@HN1C	PE_1786@N31	2.7692	159.3289
ASP_115@OD1	PE_1852@HN1C	PE_1852@N31	2.7951	155.9383
GLU_28@OE2	PE_1855@HN1B	PE_1855@N31	2.8189	151.4784
GLU_131@OE1	PE_1858@HN1B	PE_1858@N31	2.7669	158.6081
GLU_105@OE2	PE_1765@HN1B	PE_1765@N31	2.7912	153.8374
GLU_114@O	PE_1900@HN1A	PE_1900@N31	2.8057	153.949
ASP_115@O	PE_1900@HN1A	PE_1900@N31	2.8298	153.2583
GLU_104@OE2	PS_1795@HN1C	PS_1795@N31	2.7915	156.9054
GLU_126@OE1	PE_1786@HN1A	PE_1786@N31	2.8066	153.6689
GLU_114@O	PE_1900@HN1C	PE_1900@N31	2.8192	155.6209
GLU_105@OE2	PE_1765@HN1A	PE_1765@N31	2.7869	153.4292
GLU_126@OE2	PE_1786@HN1A	PE_1786@N31	2.8079	152.4051
GLU_110@OE1	PE_1852@HN1C	PE_1852@N31	2.7746	157.2219
GLU_83@OE1	PS_1846@HN1C	PS_1846@N31	2.7967	156.3345
GLU_137@OE2	PE_1807@HN1B	PE_1807@N31	2.7762	155.6976
GLU_114@O	PE_1900@HN1B	PE_1900@N31	2.7991	152.1005
PRO_117@O	PE_1852@HN1B	PE_1852@N31	2.836	157.6542
GLU_131@OE1	PE_1858@HN1C	PE_1858@N31	2.7828	155.2136
ASP_115@O	PE_1900@HN1C	PE_1900@N31	2.832	153.9229
GLU_105@OE2	PS_1774@HN1B	PS_1774@N31	2.7823	158.8446
ASP_115@OD1	PE_1852@HN1B	PE_1852@N31	2.7874	155.2022
GLN_134@O	PE_1777@HN1A	PE_1777@N31	2.7914	151.3546
GLU_110@OE1	PE_1903@HN1B	PE_1903@N31	2.7846	155.815
ASP_115@O	PE_1900@HN1B	PE_1900@N31	2.8368	153.1363
GLU_105@OE1	PE_1765@HN1A	PE_1765@N31	2.8102	152.5451
GLU_110@OE1	PE_1852@HN1A	PE_1852@N31	2.7785	157.71
GLU_104@OE1	PS_1795@HN1A	PS_1795@N31	2.7933	156.6455
GLU_131@OE2	PE_1858@HN1B	PE_1858@N31	2.7692	158.8229
GLU_137@OE1	PE_1807@HN1B	PE_1807@N31	2.7893	157.7011
GLU_104@OE1	PS_1795@HN1B	PS_1795@N31	2.8009	157.1186
GLU_110@OE1	PE_1903@HN1A	PE_1903@N31	2.7857	154.0061
GLU_105@OE1	PE_1765@HN1B	PE_1765@N31	2.8068	151.7843
ASP_115@HB3	PE_1900@H2A	PE_1900@C32	2.8833	145.5562
GLU_105@OE2	PS_1774@HN1A	PS_1774@N31	2.7705	158.3857

GLU_131@OE2	PE_1858@HN1C	PE_1858@N31	2.7818	156.1161

Table 8a.6. *Intermolecular Hydrogen bond analysis of membrane bound NPT200-11-α-Syn complex during the MD simulation of 100 ns with membrane bilayer as acceptor and α-Syn in presence of NPT200-11 as donor*

#Acceptor	DonorH	Donor	Average Distance (Å)	Average Angle (º)
PC_1828@O33	GLN_62@HE21	GLN_62@NE2	2.7596	156.7842
PS_1804@O22	GLN_62@HE22	GLN_62@NE2	2.8233	160.733
PC_1828@O34	LYS_58@HZ3	LYS_58@NZ	2.7383	163.5847
PE_1855@O34	LYS_58@HZ1	LYS_58@NZ	2.7225	154.9471
PE_1894@O34	LYS_58@HZ2	LYS_58@NZ	2.7842	162.0989
PC_1828@O33	THR_59@HG1	THR_59@OG1	2.7111	164.8954
PS_1837@O33	SER_42@HG	SER_42@OG	2.6445	164.391
PS_1792@O12	GLY_101@H	GLY_101@N	2.8364	158.6923
PS_1813@O22	LYS_97@HZ3	LYS_97@NZ	2.7566	157.6766
PS_1813@O34	LYS_97@HZ1	LYS_97@NZ	2.7771	159.394
PS_1813@O22	LYS_97@HZ2	LYS_97@NZ	2.7619	156.8618
PS_1813@O34	LYS_97@HZ3	LYS_97@NZ	2.7758	157.065
PS_1792@O36	ASN_103@HD22	ASN_103@ND2	2.8095	158.687
PE_181@O33	LYS_6@HZ2	LYS_6@NZ	2.7642	158.9548
PE_1834@O12	LYS_80@HZ3	LYS_80@NZ	2.7723	153.3917
PE_1843@O33	LYS_80@HZ1	LYS_80@NZ	2.7625	157.5936
PE_1765@O34	LYS_102@HZ3	LYS_102@NZ	2.7699	158.007
PC_1828@O22	LYS_21@HZ2	LYS_21@NZ	2.7504	153.8161
PC_1828@O22	LYS_21@HZ1	LYS_21@NZ	2.7573	153.855
PE_1825@O22	LYS_21@HZ1	LYS_21@NZ	2.7939	151.0121
PE_1834@O12	LYS_80@HZ2	LYS_80@NZ	2.7729	153.5565
PC_1828@O22	LYS_21@HZ3	LYS_21@NZ	2.7519	153.4213
PE_1825@O22	LYS_21@HZ3	LYS_21@NZ	2.7844	150.1575
PE_1900@O33	GLN_109@HE21	GLN_109@NE2	2.7968	162.8325
PE_1765@O34	LYS_102@HZ1	LYS_102@NZ	2.7582	158.6231
PE_1891@O34	ASN_65@HD21	ASN_65@ND2	2.7818	163.559
PE_1900@O34	GLN_109@HE21	GLN_109@NE2	2.7827	156.0154
PS_1813@O36	LYS_102@HZ1	LYS_102@NZ	2.7813	157.2588
PE_1843@O33	LYS_80@HZ3	LYS_80@NZ	2.7415	159.0588
PE_1894@O34	LYS_58@HZ3	LYS_58@NZ	2.7872	162.0324
PS_1837@O33	SER_42@H	SER_42@N	2.8336	152.2118
PE_160@O33	MET_1@H1	MET_1@N	2.7538	155.5272
PE_1825@O22	LYS_21@HZ2	LYS_21@NZ	2.7892	151.0706
PE_1855@O34	LYS_58@HZ2	LYS_58@NZ	2.7183	155.3683
PE_1786@O34	GLN_134@HE22	GLN_134@NE2	2.8089	162.2512
PE_1765@O34	LYS_102@HZ2	LYS_102@NZ	2.7714	158.2258
PC_1771@O33	LYS_43@HZ1	LYS_43@NZ	2.7318	160.28
PS_1846@O33	LYS_80@HZ3	LYS_80@NZ	2.7537	156.6306
PE_1843@O33	LYS_80@HZ2	LYS_80@NZ	2.7457	158.9176
PS_1813@O36	LYS_102@HZ2	LYS_102@NZ	2.7819	155.9656
PE_1834@O12	LYS_80@HZ1	LYS_80@NZ	2.7714	151.6977
PS_1813@O35	LYS_102@HZ1	LYS_102@NZ	2.782	155.3367
PC_1828@O34	LYS_58@HZ1	LYS_58@NZ	2.7428	162.808
PS_1813@O35	LYS_102@HZ2	LYS_102@NZ	2.7879	155.9118
PE_1777@O22	TYR_133@HH	TYR_133@OH	2.7093	157.2167
PS_1813@O34	LYS_97@HZ2	LYS_97@NZ	2.7896	158.4438
PS_1831@O12	GLN_99@HE22	GLN_99@NE2	2.8261	152.4624

PS_2017@O33	ASN_65@HD22	ASN_65@ND2	2.8311	160.549
PS_1813@O22	LYS_97@HZ1	LYS_97@NZ	2.7495	154.1989
PS_1813@O35	LYS_102@HZ3	LYS_102@NZ	2.781	157.0405

Table 8a.7. *Intermolecular Hydrogen bond analysis of membrane bound NPT200-11-α-Syn complex during the MD simulation of 100 ns with α-Syn in presence of NPT200-11 inhibitor as acceptor and membrane bilayer as donor*

#Acceptor	DonorH	Donor	Average Distance (Å)	Average Angle (º)
GLU_28@OE2	PE_1855@HN1B	PE_1855@N31	2.8078	158.0098
GLU_28@OE1	PE_1855@HN1A	PE_1855@N31	2.7624	150.6545
GLU_28@OE2	PE_1855@HN1A	PE_1855@N31	2.8284	152.7063
GLU_131@OE2	PE_1858@HN1C	PE_1858@N31	2.7694	157.6854
GLU_123@OE1	PE_1852@HN1A	PE_1852@N31	2.7778	155.2567
GLU_123@OE1	PE_1852@HN1B	PE_1852@N31	2.7729	155.8539
ASP_115@OD2	PE_1903@HN1C	PE_1903@N31	2.791	154.6049
GLU_28@OE1	PE_1855@HN1B	PE_1855@N31	2.7632	147.5975
GLU_139@OE1	PE_1807@HN1C	PE_1807@N31	2.7636	156.7936
ASP_115@OD2	PE_1903@HN1B	PE_1903@N31	2.7876	155.2142
GLU_131@OE1	PE_1858@HN1C	PE_1858@N31	2.7836	157.1884
GLU_123@OE1	PE_1852@HN1C	PE_1852@N31	2.7828	154.8755
GLU_105@OE2	PS_1774@HN1C	PS_1774@N31	2.8123	158.0541
GLU_105@OE1	PS_1774@HN1B	PS_1774@N31	2.7921	156.3819
GLU_131@OE2	PE_1858@HN1B	PE_1858@N31	2.7663	157.9374
ASP_115@OD2	PE_1903@HN1A	PE_1903@N31	2.7741	155.9963
GLU_110@OE1	PE_1903@HN1A	PE_1903@N31	2.793	157.2733
THR_81@O	PS_1897@HN1A	PS_1897@N31	2.8082	152.5406
GLU_105@OE1	PS_1774@HN1C	PS_1774@N31	2.8014	156.4133
GLU_139@OE1	PE_1807@HN1B	PE_1807@N31	2.7575	156.5555
GLU_131@OE1	PE_1858@HN1B	PE_1858@N31	2.7833	158.4281
GLU_104@OE1	PE_1765@HN1B	PE_1765@N31	2.7743	157.4288
GLU_104@OE2	PE_1765@HN1B	PE_1765@N31	2.779	154.7821
GLU_104@OE1	PE_1765@HN1C	PE_1765@N31	2.7753	155.0042
GLU_104@OE1	PE_1765@HN1A	PE_1765@N31	2.7764	154.4835
GLU_123@OE2	PE_1852@HN1C	PE_1852@N31	2.7991	156.0454
ASP_115@OD1	PE_1903@HN1C	PE_1903@N31	2.8183	155.1337
GLU_104@OE2	PE_1765@HN1A	PE_1765@N31	2.7863	154.4847
GLU_139@OE1	PE_1807@HN1A	PE_1807@N31	2.7673	155.7518
GLU_131@OE1	PE_1858@HN1A	PE_1858@N31	2.7666	157.9906
GLU_131@OE2	PE_1858@HN1A	PE_1858@N31	2.7726	157.2299
GLU_105@OE2	PS_1774@HN1B	PS_1774@N31	2.8315	155.6752
GLU_83@OE2	PE_1888@HN1B	PE_1888@N31	2.7937	158.4902
LYS_21@HE3	OL_1826@H3S	OL_1826@C13	2.8759	148.0821
THR_81@O	PS_1897@HN1B	PS_1897@N31	2.8189	156.0295
THR_81@O	PS_1897@HN1C	PS_1897@N31	2.8161	153.54
TYR_136@O	PE_1768@HN1B	PE_1768@N31	2.8145	153.1935
GLU_110@OE1	PE_1903@HN1B	PE_1903@N31	2.7974	155.5132
TYR_136@O	PE_1768@HN1C	PE_1768@N31	2.811	151.9828
PRO_138@O	PE_1768@HN1A	PE_1768@N31	2.8287	153.2867
ALA_140@O	PE_1807@HN1B	PE_1807@N31	2.7672	156.9534
GLU_123@OE2	PE_1852@HN1A	PE_1852@N31	2.7862	156.0031
GLU_104@OE2	PE_1765@HN1C	PE_1765@N31	2.7879	154.9595
ASP_115@OD2	PE_1900@HN1C	PE_1900@N31	2.8062	157.6308

ASP_115@OD1	PE_1903@HN1A	PE_1903@N31	2.7932	155.7144
GLU_83@O	PE_1888@HN1A	PE_1888@N31	2.8146	149.5523
ASN_65@OD1	PS_2017@HN1A	PS_2017@N31	2.8345	153.695
GLN_134@OE1	PE_1786@HN1C	PE_1786@N31	2.8006	155.1147
GLU_105@OE2	PS_1774@HN1A	PS_1774@N31	2.8132	158.7524
GLU_110@OE1	PE_1903@HN1C	PE_1903@N31	2.7868	158.2435

8a.4.12. Binding Free Energy (BFE) analysis:

FastDRH, is a user-friendly and multifunctional online platform to calculate MM/PB (GB) SA free energy and multiple poses based per-residue energy decomposition analysis [262]. The BFE of the NPT100-18A+α-Syn and NPT200-11+α-Syn complexes were calculated using FastDRH which is based on computational docking and MM/GBSA methods. The BFE determined for the NPT100-18A+α-Syn and NPT200-11+α-Syn complexes along with the various energy terms, were summarized in **Table 8a.8**. From **Table 8a.8**, it can be seen that the NPT200-11+ α-Syn complex (ΔG_{bind}= -31.86 kcal/mol) was energetically more favourable than the NPT100-18A+ α-Syn complex (ΔG_{bind} = -21.6 kcal/mol). It is also seen that all the derived components (VDW = van der Waals contribution; ELE = electrostatic energy; GB = the electrostatic contribution to the polar solvation free energy, SA= Surface Area) from the BFE analysis significantly contributed to the binding of α-Syn protein and inhibitors (NPT100-18A and NPT200-11).

Table 8a.8. *Binding free energies (kcal/mol) and its derived components of α-Syn protein and inhibitor (NPT100-18A and NPT200-11) complexes obtained using FastDRH server*

Components	(NPT100-18A+ α-Syn) complex (kcal/mol)	(NPT200-11+α-Syn) complex (kcal/mol)
VDW	-33.81	-42.31
ELE	0	0
GB	15.49	14.35
SA	-3.24	-3.93
Total ($\Delta G_{binding}$)	-21.6	-31.86

VDW = van der Waals contribution; ELE = electrostatic energy; GB = the electrostatic contribution to the polar solvation free energy, SA= Surface Area and BFE ($\Delta G_{binding}$).

8a.5. Conclusion:

In this study, the effect of the two peptidomimetic compounds (NPT200-11 and NPT100-18A) on the interactions between the α-Syn and membrane were demonstrated using all-atom MD simulation. The properties of HOMO-LUMO band gap, ionization potential, electron affinity and electronegativity values were evaluated to determine the electron donation and acceptance

ability of the inhibitor compounds in response to the environment. The calculations showed that the NPT100-18A and NPT200-11 possess a large comparable MO band gap, which are essential to predict their possible level of stability. Both inhibitors showed intermediate electrostatic potential. In general, it is noted that the penetration of α-Syn into the membrane rapidly influences its transition from α-helical to a coiled structure. This penetration also aids in the incorporation of additional free α-Syn monomers into the complex, which causes phospholipids to displace and oligomers to form in the membrane. In our study, α-Syn in the presence of peptidomimetic inhibitors, adopts well-defined α-helical structures during its interaction with lipid membranes, which inhibits the transition of the α-helical secondary structure into a coiled structure. RMSD of Cα atoms and RMSF analyses indicated that α-Syn in the presence of inhibitors shows more stability and lower flexibility of the conformational ensembles. The secondary structural content analysis showed that α-Syn in the presence of inhibitors exhibited higher α-helical and lower β-sheets content. This suggests that this addition of inhibitors plays a significant inhibitory role in the secondary structure formation required for the aggregation mechanism. In the presence of peptidomimetic inhibitors, it was observed that the number of intermolecular hydrogen bonds between the different regions of α-Syn and membrane was relatively higher. The center of the mass distance between NAC and the C-terminal was observed to undergo change to a greater extent than the center of mass distance between other regions. The results of this work on α-Syn-membrane interactions in the presence of the two peptidomimetic inhibitors may help in the development of a disease modifying strategy for treating PD and other neurodegenerative diseases.

Chapter 8b

In silico investigation on the structural insights into the binding of Squalamine and Trodusquemine inhibitors with membrane-bound α-Synuclein

In silico investigation on the structural insights into the binding of Squalamine and Trodusquemine inhibitors with membrane-bound α-Synuclein

8b.1. Abstract:

PD and its associated symptoms are tightly linked to the self-assembly of α-Syn. Aminosterols are naturally occurring substances that were first found in dogfish sharks. They are composed of a fused sterol connected to a polyamine side chain. Aminosterols are a family of naturally occurring compounds that have been studied for a variety of medicinal uses, including as efficient protein aggregation modulators. One such aminosterol compound is Squalamine and its derivative Trodusquemine. Squalamine is a naturally occurring chemical substance with established antiviral and anticancer properties and its profound impact on the α-Syn aggregation both *in vivo* and *in vitro* is well studied. By examining its interaction with lipid vesicles, which are known to encourage nucleation, it can signify the mechanism of action of Squalamine. The Squalamine molecule is believed to displace α-Syn from the surfaces of the lipid vesicles, therefore preventing the initial steps in the process of aggregation. Additionally, Squalamine molecule reduces the harmful effects of α-Syn oligomers in human neuroblastoma cells by preventing them from interacting with lipid membranes. Trodusquemine inhibits α-Syn aggregation by suppressing both the lipid-induced nucleation and fibril amplification processes. Computational investigation of the conformational changes of membrane-bound α-Syn in the presence of Squalamine and Trodusquemine inhibitor molecules**.** MD trajectory analysis was carried out to study the structural change of the α-Syn-Squalamine conformers as a function of simulation time. The percentage of the secondary structural components of α-Syn-Squalamine and α-Syn-Trodusquemine complexes were determined. Optimization of small molecule inhibitors (Squalamine and Trodusquemine) was carried out using DFT analysis. Additionally, the values of electrophilicity (***ω***), nucleophilicity (N), Electron affinity (EA) and ionization potential (IP) were calculated. The docking of α-Syn-Squalamine and α-Syn-Trodusquemine complexes revealed the binding sites and the best structure was selected based on the highest docking vina score (-5.8 and -5.6) respectively and the contact residues were listed. From the conformational snapshots of the α-Syn-Squalamine complex, it was evident that the α-Syn remained stable maintaining its integrity throughout the simulation. The α-helical content was found to be retained from the secondary structural content analysis. The ***ω*** and N of Squalamine and Trodusquemine molecule were calculated to be -0.84, -0.68 and 3.25, 3.18 respectively. Our findings suggests that in the presence of Squalamine inhibitor

molecule, α-Syn adopts helical conformation that ensures the stability and may indicate that the Squalamine molecule causes gradual displacement of α-Syn across different regions within the lipid membrane while its derivative Trodusquemine showed higher binding affinity towards α-Syn that might stabilizes the conformation and might play a significant role in inhibiting its interaction with the membrane.

8b.2. Introduction:

PD is characterized by presence of LB consisting of aggregated forms of α-Syn [519]. The abnormal misfolding, accumulation, and depositing of α-Syn into pathogenic aggregates plays a central role in the pathogenicity of the PD [519, 520]. Extensive investigations on PD conditions have led to the availability of symptomatic treatments. In recent times, a number of chemicals, primarily aromatic in nature, have been discovered that target the production of amyloid and α-Syn self-assembly [521]. It has been very difficult to develop strategies that effectively suppress the formation of α-Syn aggregates and the toxicity that goes along with them because the aggregation mechanism of the α-Syn protein is very complex and influenced by external factors like temperature, pH, and surface contact [522]. Particularly, phospholipid binding has been shown to accelerate the formation of fibrils [523]; moreover, it has been shown that this acceleration is attained by strengthening the initial primary nucleation phase of the aggregation process [25]. Considering the available information, it was determined to investigate into the possibility of substances that might change α-Syn's binding to lipid membranes being useful in blocking its aggregation. In the light of this work, a steroid-polyamine conjugated molecule, Squalamine was introduced [524], as initially it was discovered in *Squalus acanthias* [525], and has been characterized as an inhibitor with anti-microbial [521,526, 527] and anti-angiogenic [528] effects. When it binds to the internal part of the plasma membrane, Squalamine functions as a lipid carrying positive charge and having high affinity towards anionic lipids to undergo destabilization of protein–lipid interaction [529-531]. This has an impact on the initiation of α-Syn aggregation [25]. As α-Syn was incubated with lipid membrane and Squalamine molecule, the soluble monomer's random coil shape appeared, but the protein's usual α-helical structure was lost [521]. The N-terminal of α-Syn interacted with the lipid vesicle, while the C-terminal of α-Syn showed a weak association with Squalamine, according to nuclear magnetic resonance (NMR) research. However, NMR analysis showed a decrease in the interaction between α-Syn protein and Squalamine when they were combined, without any indication of their bond [521]. These findings suggest that Squalamine molecule competes for the sites of binding on the surface of the lipid structure,

thereby Squalamine may decrease the interaction of α-Syn with the phospholipid membrane. Another interesting fact is that Squalamine modifies the first stages of α-Syn aggregation, which displaces α-Syn from lipid membranes [521,532,533]. In an A53T α-Syn transgenic mouse model for experimental PD, gum mobility was restored by oral Squalamine [534]. Results from a phase 1 clinical trial assessing the effectiveness in PD dementia are being analysed [535], and a Squalamine derivative called ENT-01 showed promise in treating constipation in PD patients [536].Consequently, by reducing the quantity of oligomers bonded to the membranes, Squalamine mitigates α-Syn aggregation and oligomeric-mediated toxicity [25,533]. Additionally, the drug increased the motility capabilities of a *Caenorhabditis elegans* model of PD and greatly reduced the amount of intracellular inclusions without affecting the expression of α-Syn [25]. Trodusquemine, often referred to as MSI-1436, is one such molecule within a class of cationic amphipathic aminosterols that have been extensively researched in animal models and human trials for the treatment of obesity, anxiety, and cancer [537, 538]. Trodusquemine, a structurally comparable blood brain barrier-permeable chemical, is being developed for clinical trials. It has also shown the capacity to remove α-Synuclein and its oligomers from the membrane, preventing its lipid-induced aggregation in vitro and in a C. elegans model of PD [521]. The impact of other naturally occurring aminosterol compounds was associated with Squalamine [539] on the development and characteristics of α-Synuclein aggregates both *in vitro* and *in vivo*. Trodusquemine was first identified as a secondary aminosterol in dogfish shark liver, along with six other similar chemicals, such as Squalamine [539]. Additionally, it has been demonstrated to possess the ability to penetrate the blood-brain barrier, which is a crucial characteristic for any therapeutic molecule intended for the management of neuropathic illnesses [540]. Furthermore, Trodusquemine has been demonstrated to have no discernible effect on intact tissues while promoting regeneration in a variety of vertebrate tissues and organs after injury [541].With a spermine moiety in place of a spermidine one on the side chain, Trodusquemine has a higher positive charge than Squalamine while nevertheless having the same parent structure. With the structural resemblance between Trodusquemine and Squalamine, as well as prior findings indicating that the positively charged Trodusquemine may improve its capacity to lower negative electrostatic surface charges on intracellular membranes [542, 529]. The impact of Trodusquemine on the α-Syn aggregation kinetics was analyzed *in vitro* under experimental settings previously employed to examine discrete microscopic stages in the α-Syn aggregation process in the absence of any aminosterol [152, 543]. Trodusquemine suppresses the formation of aggregates, but we have also shown that it prevents α-Syn from secondary nucleating, which lowers the aggregates' rate of growth.

The significant protective benefits of Trodusquemine in both cultured cells and a *C. elegans* model of PD can be explained by the decrease of both of these nucleation processes by Trodusquemine, which will also significantly lower the quantity of potentially dangerous aggregates. Trodusquemine treatment also increases the lifetime of the PD worms, much more than that of the control animals and somewhat more than that of Squalamine. All of these findings point to the potential advantages of Trodusquemine, which can cross the blood-brain barrier, in the context of human synucleinopathies. These advantages might include disease modification and tissue regeneration, as well as a better understanding of the onset and progression of these conditions. In this study, we aim to further understand the effect of the binding of the Squalamine inhibitor molecule at the N-terminal of α-Syn and its subsequent aggregation patterns in the membrane-bound state. Also, we have studied the effect of Trodusquemine inhibitor on α-Syn protein using docking models and analysed in association with membrane systems using LigPlot analysis.

8b.3. Materials and Methods:

8b.3.1. Molecular Docking of the α-Synuclein and inhibitor molecules (Squalamine and Trodusquemine):

8b.3.1.1. Preparation of the receptor WT α-Synuclein:

The 3-D structure of human bound micelle WT α-Syn was retrieved from RCSB database [457] (PDB ID:1XQ8) [544]. Further molecular docking was performed using this receptor molecule.

8b.3.1.2. Optimization of the inhibitor molecules (Squalamine and Trodusquemine):

DFT formalism were considered to characterize the ground state structure of the Squalamine and Trodusquemine compounds without any geometry constraint (**Figure 8b.1** and **Figure 8b.2**). We identified the compound as a neutral ligand with singlet ground state geometry. B3LYP hybrid functional [287] were used in conjunction with Def2-TZVP basis set [288, 289] to optimize the compounds without any geometry constraint. Dispersion effect was included by considering D3 version of Grimme's damping dispersion correction [290]. To mimic the solvent environment, we considered CPCM for aqueous environment with ε = 80.0 [291]. Frequency calculations were carried on top of optimized geometry at the same methodology as stated above to characterize the nature of stationary point. All calculated frequencies were identified as real vibrational frequencies. All calculations were carried out with Gaussian 16 version C.01 suit of program [292]. NBO analysis were performed on optimized Squalamine

compound (B3LYP + D3/Def2TZVP, CPCM) in order to in-depth understanding of nature of frontier MO as implemented in Gaussian 16 program [513].

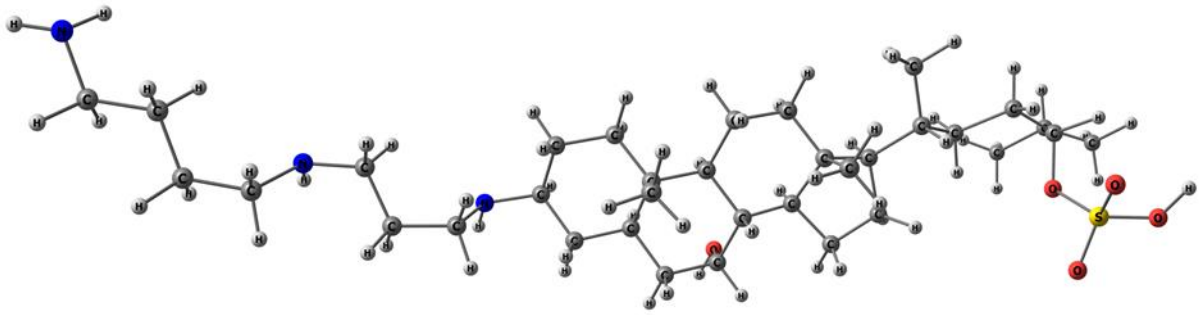

Figure 8b.1. *B3LYP + D3/Def2TZVP, CPCM calculated singlet optimized structure of Squalamine complex considered in this study*

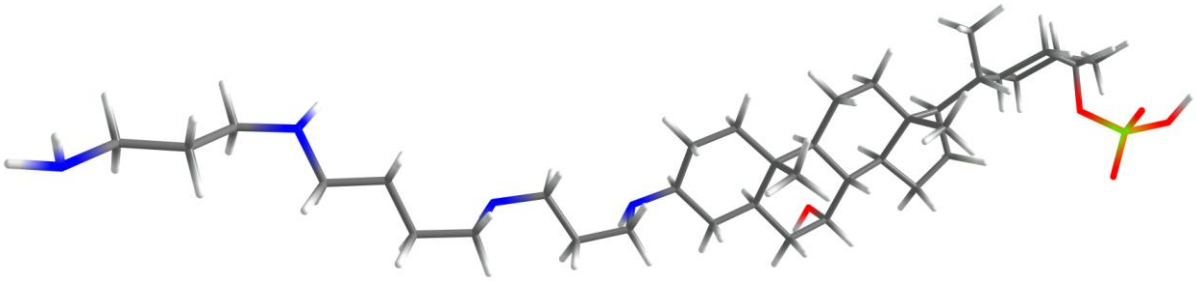

Figure 8b.2. *B3LYP + D3/Def2TZVP, CPCM calculated singlet optimized structure of Trodusquemine complex considered in this study.*

8b.3.2. Docking of α-Synuclein protein and inhibitor molecules (Squalamine and Trodusquemine):

Using CB-Dock2, an online docking service [240], the α-Syn protein that was obtained from the PDB was then docked with Squalamine and Trodusquemine complex. CB-Dock2 server provides several models of docked complexes based on structure-based molecular docking. The first complex structure among the model structures was selected for further study based on the number of binding pockets and docking score. Also, the binding site and the contact residues involved in the docking were listed by the server results.

8b.3.3. Formation of membrane bound α-Synuclein protein and inhibitor molecules (Squalamine and Trodusquemine):

Using the CHARMM GUI server, the docked complex of α-Syn and Squalamine molecule was uploaded to initiate the membrane bilayer assembly process. The hetero chain residue is read using the CHARMM general force field, and the PPM server was used to estimate the protein's

initial orientation with respect to the lipid/water interface [220]. The web-based graphical interface CHARMM-GUI was used to prepare the input files for MD computations [220]. The complex was constructed as mentioned in section **8a.3.4.**

8b.3.4. Setup for MD simulation:

The Amber 18 software [205,227] was used to run a MD simulation with the ff99SBildn force field [220]. The MD simulation protocol used for this complex using the module as mentioned in section **8a.3.4.**

8b.3.5. Binding Free Energy (BFE) analysis:

The BFE of the α-Syn in the presence of inhibitor molecules Squalamine and Trodusquemine were determined using FastDRH (http://cadd.zju.edu.cn/fastdrh/), a web server to predict the BFE, based on computational docking and MM/GBSA methods [262]. The BFE calculation was performed as mentioned in section **8a.3.7.**

8b.4. Results and Discussions:

8b.4.1. Density Functional Theory Calculation of Squalamine and Trodusquemine molecules:

The inherent ligand properties of a particular molecule can be interpreted from the MO energies of the frontier MO analysis as it reflects their key reactivity profile. To understand the overall chemical reactivity of the Squalamine molecule, we perform DFT study with help of first frontier MO analysis. Noted that these types of analysis are highly beneficial to portrait electron donation or acceptance ability. Accordingly, we analyze electronic environment property from the first highest occupied and lowest unoccupied MO (HOMO and LUMO respective) orbital (as they are highly reactive to take part in chemical reactivity) to investigate donor and acceptor ability to get an idea how Squalamine will react in protein environment. Additionally, we also perform MESP analysis to probe an impression for average possible electrophilic and nucleophilic regions delocalize overall the whole molecule. The MESP offers valuable insights into the arrangement of electrostatic charges within a molecule. It serves as a visual depiction of the electrostatic potential energy stemming from the distribution of electrons within a molecule in relation to a specific point in space. MESP proves instrumental in investigating the reactivity and binding properties of molecules, shedding light on their interaction dynamics. Based on the performed NBO partitioning analysis, we characterized the first five HOMO and LUMO orbitals to predict the nature of donation and acceptance properties of the Squalamine complex as shown in **Figure 8b.3(A)**. Through the conducted NBO partitioning analysis, we investigated the first five highest occupied and lowest unoccupied MO (HOMO and LUMO,

respectively) orbitals to anticipate the donation and acceptance properties of the Trodusquemine complex, as illustrated in **Figure 8b.4(A)**. Upon examining the positions of all five HOMOs, it becomes evident that Trodusquemine ligand primarily functions as a sigma-donor ligand by nature. In HOMO, HOMO-1, HOMO-2, and HOMO-3, the sigma-symmetric lone pair orbitals of the extended amine framework is exclusively present. Conversely, the sigma-donor region in HOMO-4 is notably delocalized, particularly within the phenanthrene framework. On the other hand, inspections of unoccupied orbitals revels that the corresponding LUMOs exhibit exclusively a sigma-antibonding character (in case of all five LUMO), which particularly delocalized either in SO_3H group or whole phenanthrene framework. Further, we also evaluated the distributed electron density in the whole Squalamine molecule from MESP as it defines the total charge distribution and accordingly interpret probable coupling interaction with respect to the neighboring environment, **Figures 8b.3(B)** and **8b.4(B)** [511, 514]. From DFT optimized structure, we generated Self-consistent field (SCF) total electron density to calculate MESP map. Inspection from **Figure 8b.3(B)** and **Figure 8b.4(B)** defines, the electron donation region delocalizes over the SO_3H and isobutyl group and extended amino framework.

Electron donation and acceptance ability can be further probed by evaluating the corresponding values of the N and ω indices respectively as they can interpret the electronic behavior with respect to the nearby environment. N and ω values can be evaluated using the following equations, $N = E_{HOMO} - E_{HOMO\ (TCNE)}$ [512] and $\omega = \mu^2/2\eta$ where $\mu = (E_{HOMO} + E_{LUME})/2$ and $\eta = (E_{HOMO} - E_{LUMO})$ respectively as shown in **Table 8b.1** [515-517]. In addition, we also calculated HOMO-LUMO band gap ($\Delta E_{HOMO\text{-}LUMO}$), IP, EA and electronegativity values of the Squalamine and Trodusquemine compounds as listed in **Table 8b.1**. We estimated the adiabatic IP and EA, by subtracting the Gibbs free energy values from its neutral closed shell one to the corresponding cationic and anionic species respectively (which can be calculated by subtracting and adding one electron respectively). The significantly stable HOMO-LUMO energy gap observed in Trodusquemine suggests the potential isolation for its experimental realization. In fact, its band gap value is substantially higher than the corresponding Squalamine complex (~11 kcal/mol). Additionally, the calculated ionization potential indicates Trodusquemine's strong electron-donating ability, nearly comparable to the first ionization potential of lithium (124.5 kcal/mol).

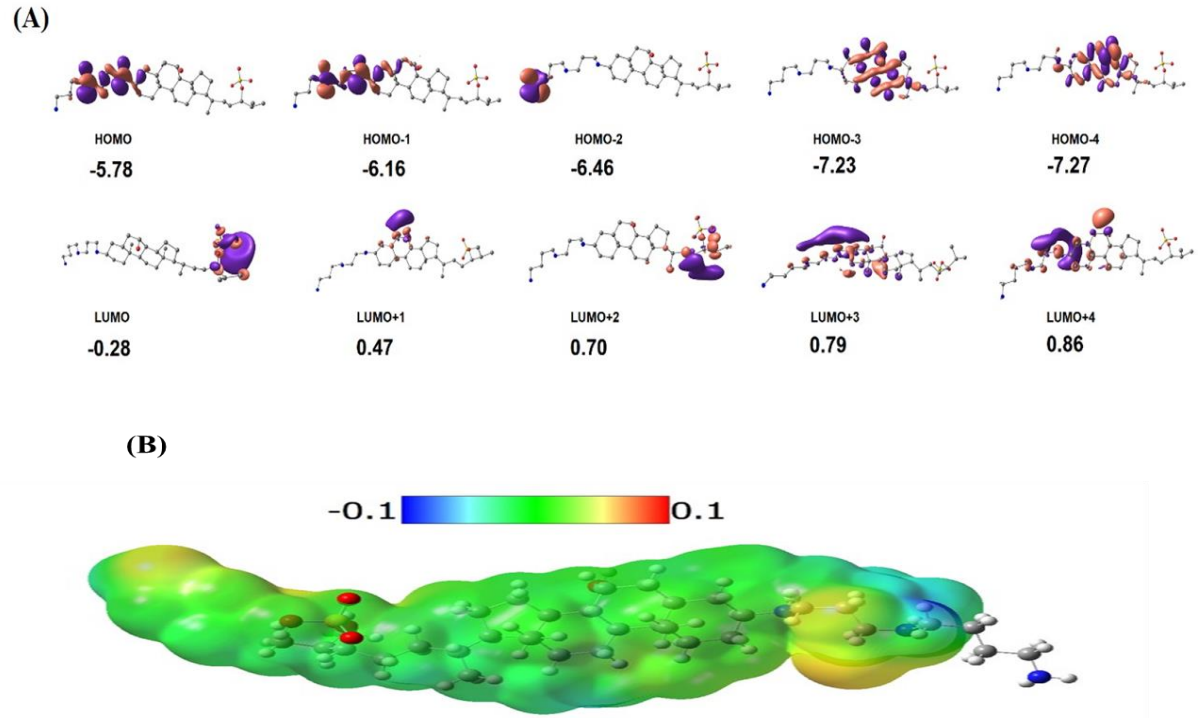

Figure 8b.3. (A) *Energies (in eV) of first five highest occupied (HOMO, HOMO-1, HOMO-2, HOMO-3, and HOMO-4) and lowest unoccupied (LUMO, LUMO+1, LUMO+2, LUMO+3 and LUMO+4) frontier MO of Squalamine complex calculated in B3LYP+D3/def2-TZVP (/CPCM) level of theory.* ***(B)*** *Calculated electron density plot from electrostatic potential map (ESP) for Squalamine complex at B3LYP+D3/def2-TZVP (/CPCM) level of theory*

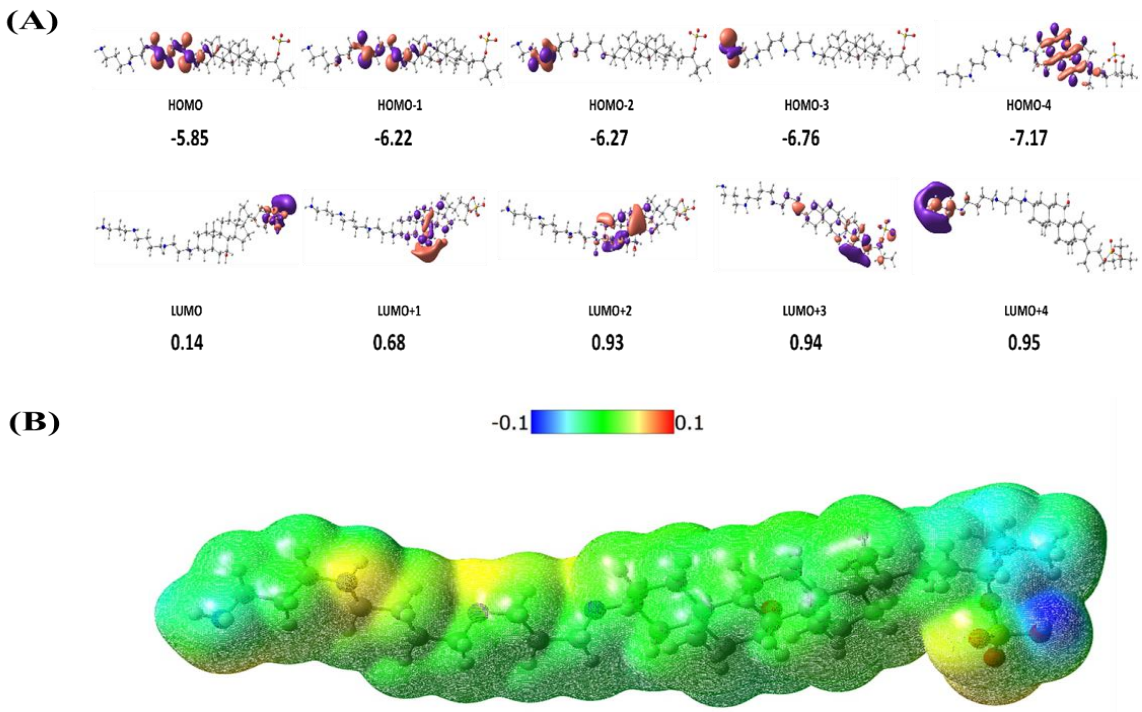

Figure 8b.4. *(A) Energies (in eV) of first five highest occupied (HOMO, HOMO-1, HOMO-2, HOMO-3, and HOMO-4) and lowest unoccupied (LUMO, LUMO+1, LUMO+2, LUMO+3 and LUMO+4) frontier MO of Trodusquemine complex calculated in B3LYP+D3/def2-TZVP*

(/CPCM) level of theory. ***(B)*** *Calculated electron density plot from electrostatic potential map (ESP) for Trodusquemine complex at B3LYP+D3/def2-TZVP (/CPCM) level of theory.*

Table 8b.1. *Calculated values of nucleophilicity (N, eV) and electrophilicity (**ω,** eV) indices, ionization potential (IP, in kcal/mol), electron affinity (EA, in kcal/mol) and HOMO-LUMO band gap ($\Delta E_{HOMO-LUMO}$, in kcal/mol) for Squalamine molecule and Trodusquemine*

Molecule	N	ω	IP	EA	$\Delta E_{HOMO-LUMO}$
Squalamine	3.25	-0.84	122.5	51.9	-126.9
Trodusquemine	3.18	-0.68	121.8	54.8	-138.3

8b.4.2. Docking study of α-Synuclein+ inhibitor molecules (Squalamine and Trodusquemine):

The 3-D structure of full-length α-Syn monomer was obtained from RCSB database (1XQ8) consisting of 140 amino acid residues. This model structure was used for docking with small molecule inhibitors (Squalamine and Trodusquemine) using CB-Dock2 server. In a recent study, this protein was used as a receptor molecule (target protein) for molecular blind docking of small molecule inhibitors (Squalamine and Trodusquemine) [521]. We have tabulated all the binding sites, cavity volume and contact residues of Squalamine and Trodusquemine molecules targeting α-Syn were tabulated in **Table 8b.2** and **Table 8b.3**. The binding sites at C-terminal of Squalamine complex was observed to have lower binding score as compared to N-terminal binding site while in case of Trodusquemine complex, the strongest binding affinity was found to be higher at the C-terminal. From **Table 8b.2 and Table 8b.3**, it was observed that the best predicted structure showed binding of Squalamine molecule to the N-terminal region of α-Syn with the highest vina score (-5.8) and cavity volume of 164 A^3 and binding of Trodusquemine molecule to the C-terminal region of α-Syn with the highest vina score (-5.6) and cavity volume of 7 A^3.

Table 8b.2. *Predicted binding sites of the (α-Syn+Squalamine) complex using CB-docking2 server including Molecular Docking Score, cavity volume and contact residues.*

Pocket ID	Docking Vina score	Cavity volume (A^3)	Contact Residues
C2	-5.8	164	ALA29 LYS32 THR33 LYS34 GLU35 GLY36 VAL37 LEU38 TYR39 VAL40 GLY41 SER42

			LYS43 THR44 LYS45 GLU46 VAL48
C1	-5.6	285	PRO117 VAL118 ASP119 ASP121 ASN122 GLU123 ALA124 TYR125 GLU126 MET127 PRO128 SER129 GLU130 GLU131 GLY132 TYR133 GLN134 ASP135 TYR136 GLU137 PRO138 ALA140

Table 8b.3. *Predicted binding sites of the (α-Syn+Trodusquemine) complex using CB-docking2 server including Molecular Docking Score, cavity volume and contact residues.*

Pocket ID	Docking Vina score	Cavity volume (A^3)	Contact Residues
C5	-5.6	7	GLU123 ALA124 TYR125 GLU126 MET127 PRO128 SER129 GLU130 GLU131 GLY132 TYR133 GLN134 ASP135 TYR136 GLU137 PRO138 GLU139 ALA140
C3	-5.5	25	PRO108 GLN109 GLU110 GLY111 ILE112 LEU113 GLU114 ASP115 MET116 PRO117 VAL118 ASP119 PRO120 ASP121 ASN122 GLU123 ALA124 TYR125 GLU126 MET127 PRO128 SER129

8b.4.3. Conformational snapshots of the (α-Synuclein+Squalamine) and (α-Synuclein+Trodusquemine) complexes:

The conformational snapshots of the complex showing the structural change in the α-Syn protein in the presence of inhibitor molecule Squalamine during the MD simulation were obtained using UCSF Chimera [306]. The snapshots were obtained at corresponding different time intervals as shown in **Figure 8b.5** and **Figure 8b.6**. From the conformational snapshots of the complex demonstrated that the non-amyloid component (NAC) domain and C-terminal regions of α-Syn protruded above the membrane surface. The N-terminal of α-Syn retained the helicity throughout the simulation and no extended helix was formed in the region (1-37)

indicating inhibition of initiation of fibrillary structures [545]. The membrane bilayer was also found to maintain its integrity throughout the simulation. The structural integrity of the membrane bilayer is retained thereby preventing the breakdown of Squalamine molecule. The Squalamine complex showed weaker interaction with the membrane bilayer during the gradual time intervals as observed in **Figure 8b.7**. The gradual movement of the α-Syn protein from within the membrane lipid core to the surface was observed as the inhibitor may compete with the protein for binding to the membrane. In the **Figure 8b.8**, it was noticed that the inhibitor molecule Trodusquemine was strongly bound to the C-terminal region of α-Syn protein even after when it is bound state with the membrane bilayer prior to MD simulation.

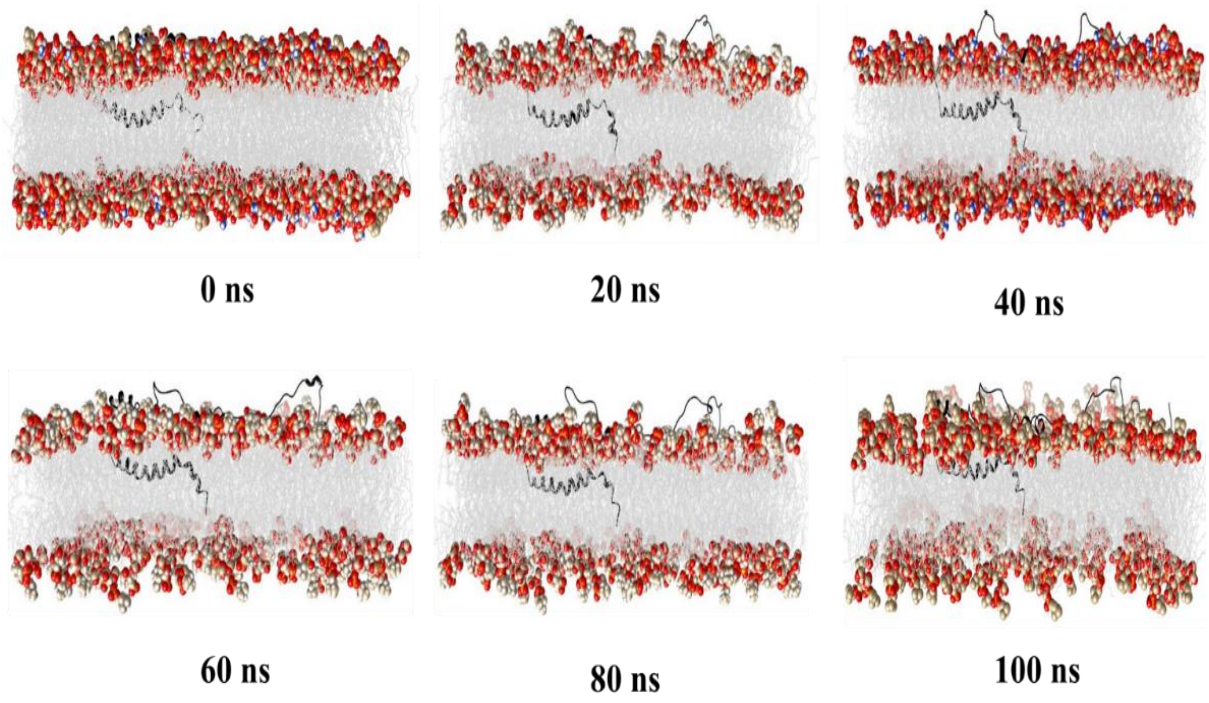

Figure 8b.5. *Conformational snapshots of membrane-bound α-Syn in the presence of inhibitor Squalamine during MD simulation*

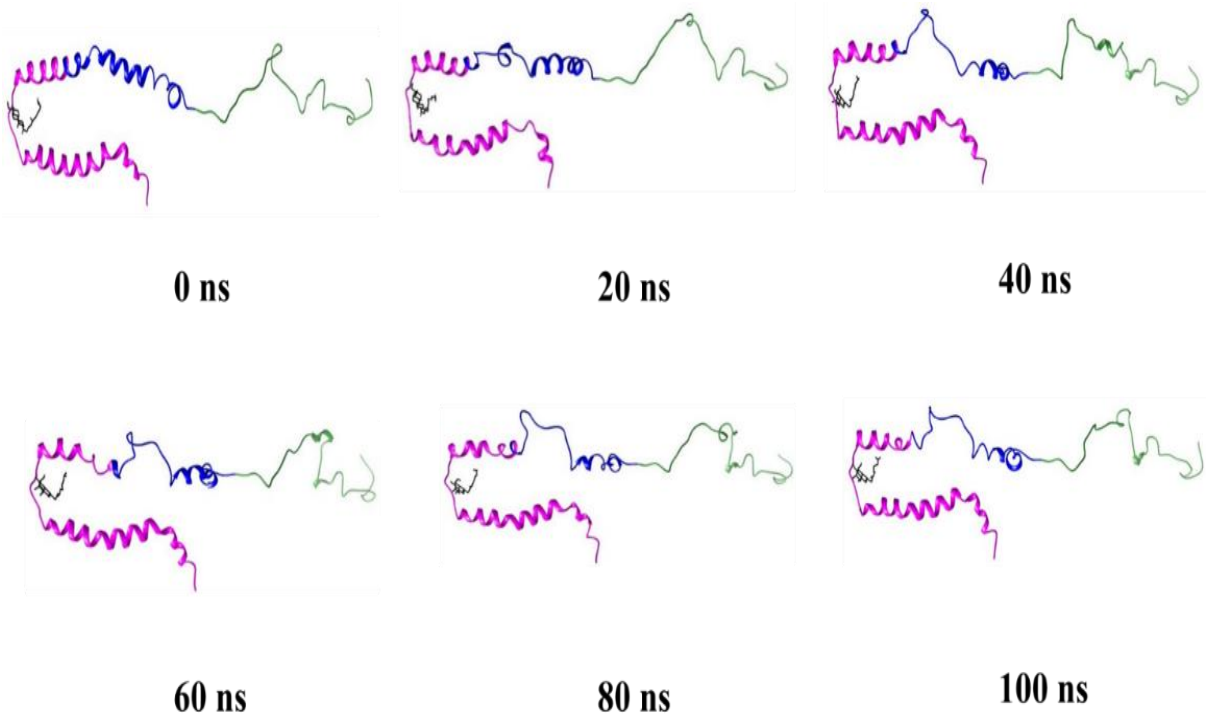

Figure 8b.6. *Conformational snapshots of membrane-bound α-Syn in the presence of inhibitor Squalamine during MD simulation (membrane hidden)*

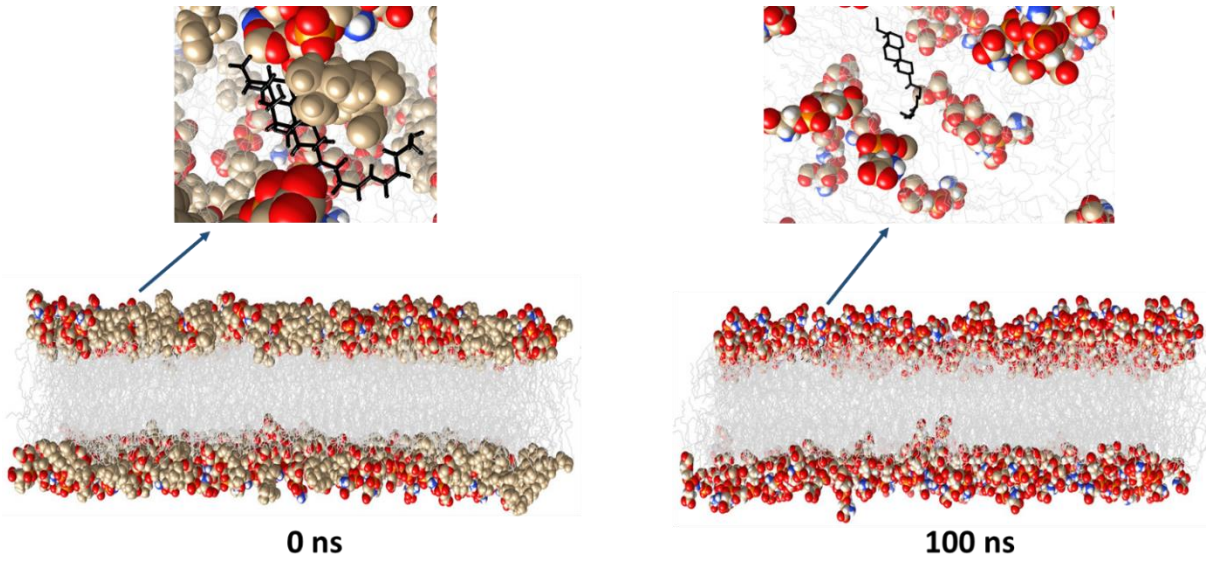

Figure 8b.7*. 3-D snapshot of membrane bound α-Syn in presence of inhibitor Squalamine during MD simulation*

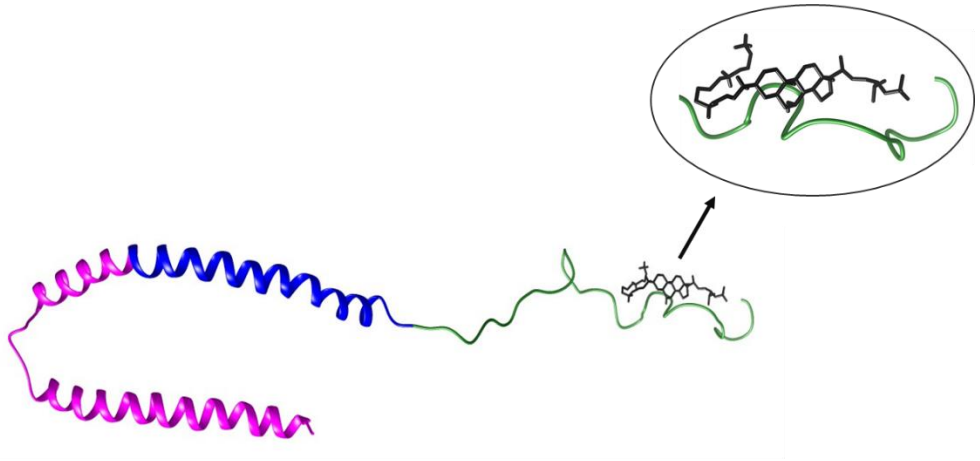

α-Syn + Trodusquemine complex

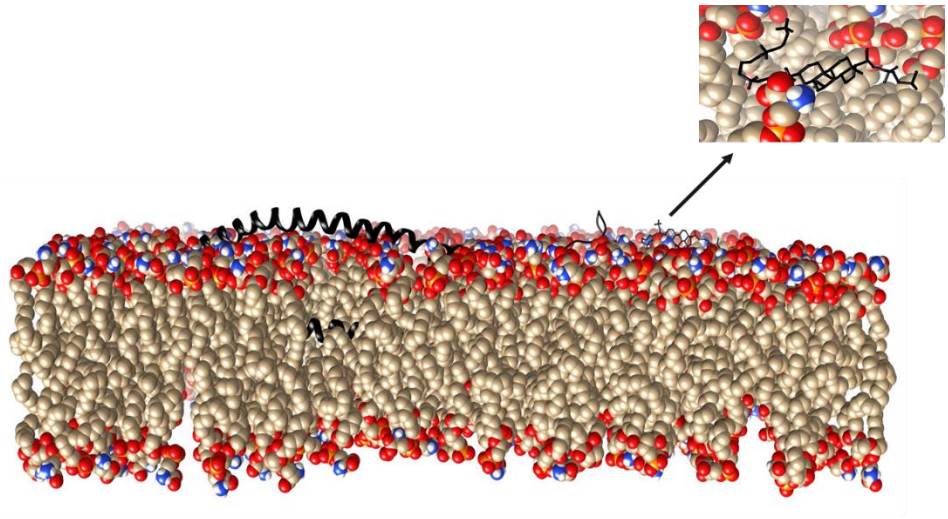

Membrane bound α-Syn + Trodusquemine complex

Figure 8b.8. *Conformational snapshots of membrane-bound α-Syn in the presence of inhibitor Trodusquemine prior to MD simulation*

8b.4.4. LigPlot analysis between the membrane-bound (α-Synuclein+Squalamine) and (Synuclein+Trodusquemine) complexes:

The interaction study between the α-Syn and inhibitor molecules (Squalamine and Trodusquemine) were analysed using Ligplot [546]. In **Figure 8b.9**, the interaction between the Squalamine molecule and α-Syn protein residues was determined. Hydrophobic interactions are shown schematically, whereas hydrogen bonds are represented by dashed lines. An arc with spokes extending towards the ligand atom in contact and vice versa represents the amino acid residues of the α-Syn protein engaged in the aforementioned interactions. In the LigPlot analysis, the interactions between the α-Syn and Squalamine molecule were identified to be Lys32, Tyr39 and Lys43. From the plot in **Figure 8b.10**, it was evident that the interaction between membrane and Squalamine molecule has been decreased suggesting the

inhibitor molecule has slightly displaces the protein from the membrane surface. The number of residues interacting between membrane bilayer and Squalamine compound at different time intervals during MD simulation was analyzed using Ligplot. In the Ligplot analysis (**Figure 8b.11**), the interaction between the α-Syn protein and Trodusquemine molecule prior to MD simulation was plotted. From the plot, it was observed that the inhibitor molecule Trodusquemine was strongly interacting with the α-Syn protein in membrane bound state.

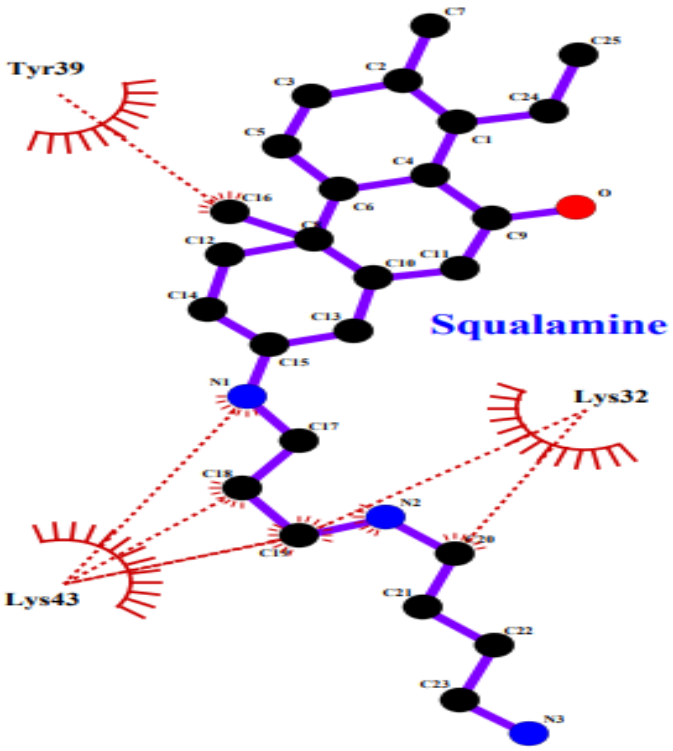

Figure 8b.9. *Ligplot analysis of membrane-bound α-Syn in the presence of inhibitor Squalamine during MD simulation*

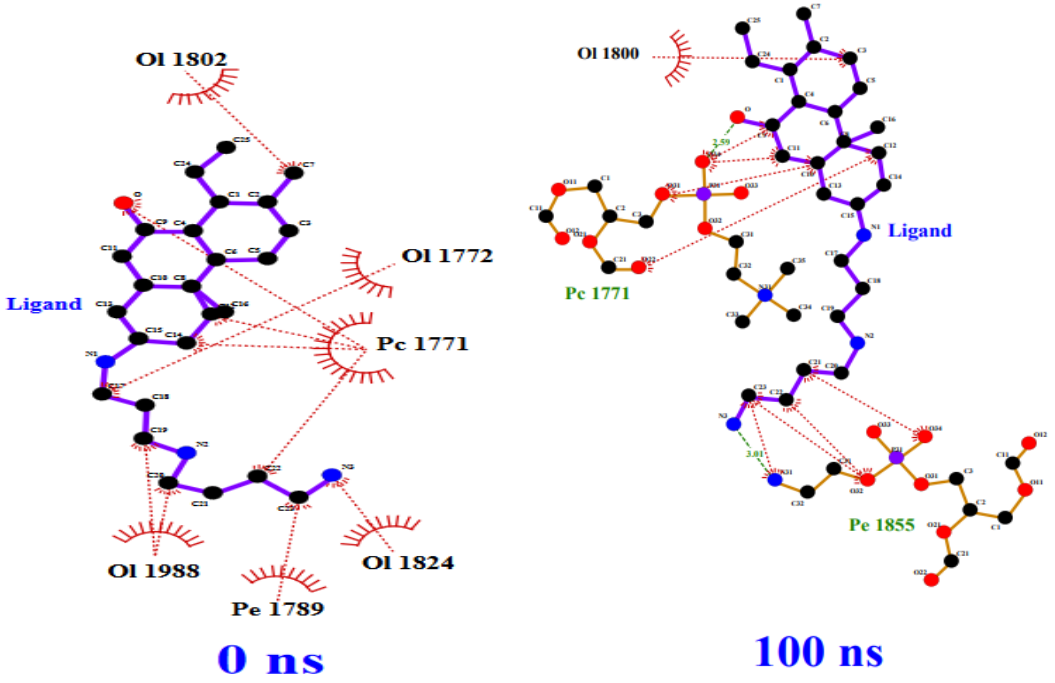

Figure 8b.10. *Ligplot analysis of the interaction between membrane bilayer and inhibitor Squalamine at different time intervals during MD simulation*

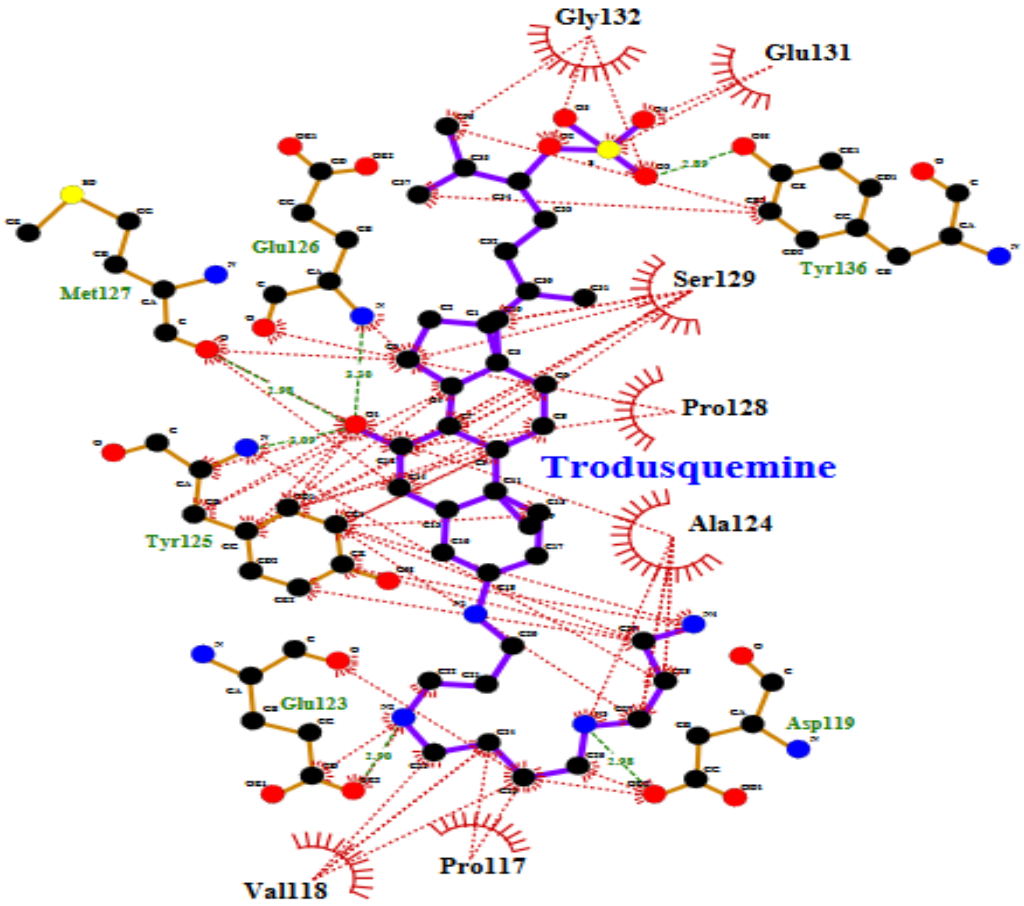

Figure 8b.11. *Ligplot analysis of membrane-bound α-Syn in the presence of inhibitor Trodusquemine prior to the MD simulation*

8b.4.5. Secondary structural content analysis:

The percentage of secondary structural content of α-Syn and inhibitor complexes (Squalamine and Trodusquemine) were calculated using YASARA software [258]. From the **Table 8b.4**, the α-helical content of the α-Syn and Squalamine complex was found to be 23.6%. The percentage of α-helical content suggest that the structure of α-Syn in the presence of Squalamine inhibitor molecule was retained. On interaction with Squalamine molecule the α-Syn inhibits the formation of beta sheet secondary structure that suggests Squalamine molecule suppresses the toxicity of the α-Syn monomer in the initial events of the aggregation. The secondary structural content for α-Syn and Trodusquemine complex was calculated prior to the MD simulation setup as tabulated in **Table 8b.5**. The percentage of alpha helix was found to be 56.7% with decreased coil conformation. From our previous work [547], it was noticed that α-Syn in the absence of inhibitor molecule contains lower helical content and higher coil content than in our findings that may contribute to the formation of conformational intermediates that are prone to aggregation by mediating the interconversion between the "extended" and "broken-helix" states. Also, it was found that the α-Syn in the absence of inhibitor contain lower alpha helical content and higher beta sheet formation as compared to α-Syn +Squalamine complex favouring the development of aggregate formation [547].

Table 8b.4. *Secondary Structural content of α-Syn+Squalamine after the simulation time using YASARA software*

COMPLEX	α-helix %	β-sheet %	turn %	Pi-helix %	3_{10} helix %	Coil %
α-Syn+Squalamine	23.6	0	25.7	0	3.6	47.1

Table 8b.5. *Secondary Structural content of α-Syn+Trodusquemine at the initial MD simulation using YASARA software*

COMPLEX	α-helix %	β-sheet %	turn %	Pi-helix %	3_{10} helix %	Coil %
α-Syn+Trodusquemine	57.6	0	5.8	0	0	36.7

8b.4.6. Binding Free Energy (BFE) Analysis:

A user-friendly and flexible online platform called FastDRH is used to determine different poses based on per-residue energy decomposition analysis and MM/PB (GB) SA free energy

[262]. BFE of α-Syn-Squalamine and α-Syn-Trodusquemine complex were determined by the use of FastDRH, a computational docking approach based on MM/GBSA techniques. In **Table 8b.6**, the different energy terms and the BFE found for the α-Syn in the presence of Squalamine and Trodusquemine inhibitor molecules. The α-Syn in the presence of Squalamine and Trodusquemine molecules showed the ΔG_{bind} value of -11.09 kcal/mol and -33.6 kcal/mol and was found to be energetically favourable. Additionally, the binding of α-Syn was greatly aided by each of the derived components (VDW, ELE, GB, and SA) from the BFE study. It is evident that the binding of Trodusquemine molecule is stronger than the Squalamine molecule to the α-Syn protein.

Table 8b.6. *Binding free energies (kcal/mol) and its derived components of α-Syn protein and inhibitor molecules (Squalamine and Trodusquemine) complexes obtained using FastDRH server*

Components	**(Squalamine + α-Syn) complex (kcal/mol)**	**(Trodusquemine+ α-Syn) complex (kcal/mol)**
VDW	-17.57	-43.86
ELE	0	0
GB	8.99	15.06
SA	-2.49	-4.77
Total ($\Delta G_{binding}$)	**-11.09**	**-33.6**

VDW = van der Waals contribution; ELE = electrostatic energy; GB = the electrostatic contribution to the polar solvation free energy, SA= Surface Area and BFE ($\Delta G_{binding}$).

8b.4.7. Salt Bridge formation:

The number and distance of salt bridges within the N-terminal, NAC, and C-terminal regions of α-Syn in presence of Squalamine inhibitor and Trodusquemine inhibitor molecules were calculated in order to determine the stability of the protein as tabulated in **Table 8b.7** and **Table 8b.8**. The presence of fibril is characterized by the formation of salt bridges and several intramolecular interactions that stabilize the α-Syn structure. The distance in angstrom (Å) between the N-terminal, NAC region, and C-terminal of the α-Syn+ Squalamine complex and α-Syn+ Trodusquemine complex interface, as well as the list of residue-residue interactions, were assessed using the ESBRI server [259]. **Table 8b.7** summarizes the presence of 8 strong intra-monomeric salt bridge that suggests stability of the α-Syn in the presence of Squalamine inhibitor molecule. Additionally, compared to other areas, the N-terminal have involved larger number of salt bridge which suggested the conformational stability of the region. On the contrary, in the **Table 8b.8** was found to have lower number of intra-monomeric salt bridge.

Consequently, it was seen that the stabilization of the α-Syn fibril maintained the salt bridge, which stabilizes the strands and prevents the fibrils from breaking down into structurally separate units.

Table 8b.7. *List of atom-atom interactions within the α-Syn+Squalamine interface from the ESBRI server*

α-Syn+Squalamine (Residue 1)				Hydrogen Bonds	α-Syn+Squalamine (Residue 2)				
Atom number	Atom name	Residue name	Residue number		Atom number	Atom name	Residue name	Residue number	Distance (Å)
106.86	NZ	LYS	6	<-->	102.70	OD1	ASP	2	2.27
106.86	NZ	LYS	6	<-->	104.17	OD2	ASP	2	0.67
109.41	NZ	LYS	12	<-->	107.18	OE1	GLU	13	3.87
104.17	NZ	LYS	21	<-->	103.54	OE1	GLU	28	2.91
109.10	NZ	LYS	23	<-->	109.89	OE1	GLU	20	2.62
99.78	NZ	LYS	34	<-->	98.63	OE1	GLU	35	2.48
105.86	NZ	LYS	80	<-->	103.90	OE1	GLU	83	2.28
86.77	NZ	LYS	96	<-->	94.04	OD1	ASP	98	3.78

Table 8b.8. *List of atom-atom interactions within the α-Syn+Trodusquemine interface from the ESBRI server*

α-Syn+Trodusquemine (Residue 1)				Hydrogen Bonds	α-Syn+Trodusquemine (Residue 2)				
Atom number	Atom name	Residue name	Residue number		Atom number	Atom name	Residue name	Residue number	Distance (Å)
102	NZ	LYS	8	<-->	98	OD1	ASP	7	1.76
102	NZ	LYS	8	<-->	98	OD2	ASP	7	3.50
102	NZ	LYS	8	<-->	104	OE1	GLU	22	3.97

8b.5. Conclusion:

In this study, the effect of Squalamine and Trodusquemine molecules on the conformational dynamics of α-Syn and Squalamine + α-Syn complex was subjected to the corresponding MD trajectory analysis. In order to understand the inhibitory effect of Squalamine and Trodusquemine molecule on lipid membrane interaction with protein, we have used phospholipid membrane that mimics the synaptic vesicle. NBO analysis of nature Squalamine

and Trodusquemine molecules of frontier MO as implemented in Gaussian 16 program. The inspection of positions in all five HOMOs reveals that Squalamine and Trodusquemine fundamentally are sigma-donor ligands where in HOMO, HOMO-1 and HOMO-2 exclusively consist of σ-symmetric lone pair orbital of the extended amine framework. On the other hand, the σ-donor region in HOMO-3 and HOMO-4 delocalized particularly in the phenantherene framework. The corresponding LUMO can be characterized as the σ-antibonding contribution between the SO_3H and isobutyl group. The band gap between HOMO and LUMO ($\Delta E_{HOMO-LUMO}$) was calculated to be -126.9 and -138.3. The DFT based binding properties such as band gap or HOMO-LUMO gap, ionization potential, electron affinity or electronegativity, offering valuable insights into the electron acceptance and donation capabilities of these compounds. Additionally, they illuminate crucial aspects such as metabolic stability, reactivity levels, and overall stability, enriching our understanding of their chemical properties. In the last context, we would like to mention that we compare the stability of Squalamine and Trodusquemine molecules in water environment. Interestingly, we obtained its impressive stability in aqueous media from calculated HOMO-LUMO gap value. We choose the solution media is water as we studied its property protein ambient which defines its relevance in water. Using blind docking method, the selected best model showed binding of Squalamine and Trodusquemine molecules to the N-terminal region and C-terminal of α-Syn respectively. The conformational changes observed from the snapshots of MD trajectories suggested subtle displacement of the protein from the membrane core without disturbing the protein's conformation or the integrity of the membrane bilayer. Also, the presence of 8 intra monomeric salt bridges within the different residues of α-Syn protein indicated the α-Syn's structural stability while Trodusquemine complex showed only 3 intra monomeric salt bridges. Majorly all the salt bridges were formed within the N-terminal region of α-Syn in the presence of Squalamine molecule. The binding free energy analysis of α-Syn protein in presence Squalamine was found to be lower as compared to the Trodusquemine molecule. Therefore, based on the initial binding affinity factors α-Syn protein in the presence of Squalamine and its derivative Trodusquemine inhibitor molecules may suggest as the potential competitors for binding to the lipid membrane and this potentiates the inhibitory role of Squalamine and its derivative Trodusquemine to act as a therapeutic agents for PD and other conditions associated with the pathogenic aggregation of α-Syn.